

Potential Well Structures in Spherical Inertial Electrostatic Confinement Devices

Ryan M. Meyer, *Member, IEEE*, Sudarshan K. Loyalka, and Mark A. Prelas

Abstract—Inertial electrostatic confinement (IEC) devices are of interest as neutron generators for many applications. Experiments by Hirsch inspired further efforts to decipher the potential distribution within IEC devices. In this paper, previous analyses of potential distributions in IEC devices are reviewed and extended. Three types of IEC systems are classified and analyzed according to the arrangement of electrodes and the species within the system. These systems are the unipolar cathode–anode (UCA) system, the bipolar cathode–anode (BCA) system, and the bipolar anode–cathode (BAC) system. Results of extensive parametric studies are reported through an efficient method for solving the Poisson’s equation. The method is benchmarked against prior computations by Hirsch and Swanson. For BCA and BAC systems, it is concluded that the double well depth (DWD) increases as the relative focusing of the secondary particle to the primary particle increases, agreeing with prior work by Momota and Miley. Although collisions are neglected in this model, and unverified energy distributions are employed, the method generally agrees with experimental observations by Gu that the DWD will increase as the perveance of the system is increased. Thus, the computations performed here serve as a valuable benchmark.

Index Terms—Electrostatic devices, fusion reactors, inertial confinement, ion accelerators.

I. INTRODUCTION

A. Possible Applications of IEC Devices

INERTIAL electrostatic confinement (IEC) devices have many potential applications, including their use as neutron generators. A few of these applications include: luggage inspection, oil well logging, medical isotope production, detection of explosives, archaeometry, forensics, breeding advanced fuels (He3), transmuting long-lived radioactive isotopes from fission reactor waste, a neutron source to drive a sub-critical fission reactor, generating power for space craft, and generating power for terrestrial needs [1]–[9]. However, much doubt has been cast on the feasibility of the latter two applications, as it has been argued that IEC devices are most likely $Q < 1$ machines [10], [11].

Medical isotopes are typically produced on site at a clinic with the use of medical isotope generators or accelerators. Isotopes used for imaging must be produced on site at the clinic due to the short half-life of typical isotopes employed for medical

imaging. The advantages of an IEC device for producing medical isotopes are that it is small, compact, and inexpensive. Such a portable neutron generator can be transported to some of the most remote places on earth in order to treat patients in a relatively inexpensive manner. Another advantage of the IEC is that the radioactivity hazard can effectively be “unplugged,” when not in use, thus, special handling, and shielding requirements are limited [12]. Of course, many of these characteristics are desirable features for a number of neutron generator applications. Experiments performed at the University of Wisconsin-Madison have generated 4–8 Bq of N13. Protons of 14.7 MeV, generated by D-He3 reactions, irradiate water flowing through the IEC reactor to produce N13. The isotope, N13, is later separated from the water [7], [8].

B. Prior Work

In light of these possible applications for the IEC devices, several experimental and theoretical studies have been conducted regarding the potential distribution within IEC devices. Of special interest is the hypothesis that alternating virtual electrodes in the interior of these devices provide the necessary confinement mechanism to make IEC devices effective fusion reactors. Hirsch conducted experiments with an ion injected spherical IEC system, and reported an unusually high neutron output (10^8 n/s for D-D reactions or 10^{10} n/s for D-T reactions) [13]. Neutron collimation data and X-ray collimation data collected by Hirsch indicated that a double potential well structure existed within his device. Electron beam probing by Swanson also indicated that a double potential structure existed [14]. However, the reliability of Hirsch’s and Swanson’s results is questionable. Proton collimation measurements by Nadler [15] indicated the existence of only a single potential well, while Langmuir and emissive probe measurements by Thorson [16] also failed to detect a double well in the potential distribution. The most recent attempt at measuring the potential distribution was performed by Gu [17]. Gu detected a double potential well using a high-resolution proton collimator. It is claimed that Gu’s results provide the most definitive evidence to date, with regard to the formation of a double potential well structure. Nevertheless, the accumulation of experimental results for potential structure measurements in IEC reactors is rather ambiguous.

Langmuir and Blodgett solved Poisson’s Equation for concentric spherical electrodes, for which a single species is emitted from the emitter and collected by the collector [18]. If the collector is surrounded by the emitter, a broad single virtual electrode forms within the collector, assuming that the species is mono-energetic and has no angular momentum, as shown in Fig. 1. Hirsch [13] modeled an ion injected IEC, in which ions

Manuscript received November 11, 2004; revised May 11, 2005. This work was supported in part by the Missouri Space Grant Consortium (MSGC) Fellowship, in part by the U.S. Department of Education’s Graduate Assistance in the Area of National Need (GAANN) Fellowship, and in part by the University of Missouri-Columbia, Huggin’s Graduate Fellowship.

The authors are with the Nuclear Science and Engineering Institute, University of Missouri-Columbia, Columbia, MO 65210 USA (e-mail: rmm346@mizzou.edu).

Digital Object Identifier 10.1109/TPS.2005.852350

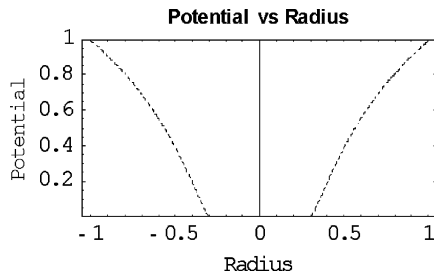


Fig. 1. Langmuir and Blodgett's solution to Poisson's Equation for concentric spherical electrodes [18].

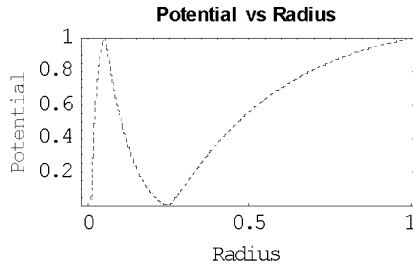


Fig. 2. Hirsch's solution to Poisson's equation for ions injected into a spherical vacuum chamber, with electrons emitted from the inner surface of the central cathode grid [13].

injected into the vacuum chamber were accelerated by a centrally located spherical cathode. In addition, it was assumed that electrons were emitted from the inner surface of the cathode grid. Hirsch approximated the ion beams as being mono-energetic and having zero angular momentum. Under these assumptions, Hirsch computed a multiple potential well structure within the cathode, as illustrated in Fig. 2.

Lavrent'ev [19], Dolan [20], and Swanson [21] developed more realistic models for electron injected devices, in which plasma was assumed to exist inside of the central anode, by accounting for energy spreads and allowing particles to have angular momentum. Solutions, computed by Swanson, indicated the formation of double potential well structures [21]. The double well hypothesis was strengthened when dynamic IEC analysis by Hockney [22] indicated that stable double potential well structures do exist.

However, further theoretical analysis was performed by Black and Klevans [23], on ion injected devices, in which electrons and ions were divided into three energy groups each. Their analysis revealed only single well formation, thus casting doubt that multiple potential wells could exist in IEC devices. Further work by Hu and Klevans [24] was aimed at finding the conditions necessary to support the multiple potential well hypotheses. However, it was concluded that the necessary conditions did not apply to Hirsch's apparatus. Thus, further questions were raised regarding the supposition that alternating virtual electrodes were responsible for the anomaly of the high fusion reaction rates recorded from Hirsch's experiments.

Recently, collisionless modeling of ion injected devices by Matsuura [25] revealed that a double potential well structure is not necessary to produce double radial peaks in the neutron production rate. Momota and Miley [26] computed the radial potential distribution for a collisionless, ion injected system. They were able to generate double potential well structures, and found

that the relative depth of a double well increased, as the relative focusing of electrons to ions improved. In addition, dynamic modeling of a collisional system by Ohnishi [27], revealed that double well formations were unstable, however, it was concluded that the transient double wells still provided a favorable environment for the acceleration of ions and the generation of neutrons.

C. Physical Characterization of IEC Devices

IEC devices are generally either cylindrical or spherical in nature. The devices focused on in this work, are the spherical variety, and will be termed spherical inertial electrostatic confinement devices (SIECs) [26]. The spherical devices consist of two spherical electrodes, with one electrode of smaller dimensions located concentrically inside of the larger electrode. The systems that have been previously referred to as electron injected systems, are constructed such that the cathode is the larger electrode, and electrons introduced to the system, either by grid emission, or by ionization, are accelerated by the positively biased central anode. If the inter-anode space is free of ions, then such a device can be referred to as a unipolar cathode-anode system (UCA). It is possible that ions are introduced within the anode of the UCA (either by electron impact ionization of background neutrals, or by emission from the inner surface of the anode grid by electron bombardment). If this is the case, then the system will contain both electron and ion current, and will be more appropriately referred to as a bipolar cathode-anode system (BCA).

If the anode is the larger electrode, the negatively biased cathode, at the center, will accelerate ions within the inter-electrode space. If it is assumed that no electrons exist within the inner region of the cathode, then such a device is termed a unipolar anode-cathode device (UAC). However, electrons may be emitted from the surface of the cathode, either by thermionic emission, or by ion bombardment of the grid. In addition, electrons will be introduced throughout the inner portion of cathode if ionizations take place within this region. If ion and electron currents exist within the cathode, then it will be referred to as a bipolar anode-cathode system (BAC).

D. Boundary Conditions

If we consider the operation of SIECs in practice, we immediately know the potential of each real electrode. In addition, we can also impose the condition that the charge density must be bounded everywhere within the region enclosed by the device. Additional conditions may be assumed, depending on the type of SIEC device in operation (unipolar or bipolar), and the energy distribution of particles within the device. These additional boundary conditions are inferred from the conditions stated above, and further physical insight. We will determine the boundary conditions for a collisionless model, and we begin by deriving the conditions for unipolar systems where the particles are mono-energetic, and have no component of their velocity in the angular direction. We then consider how these conditions are changed if the particles are given a distribution of energy, but still have no angular component. Finally, we investigate the effect of angular energy distributions on the boundary conditions. A similar approach is then applied to the bipolar systems.

Consider the UCA system in which electrons are emitted from the cathode with no kinetic energy. The centrally located anode will accelerate these electrons, and most will pass through the anode if it has a transparency η . Thus, the density of electrons increases toward the center. This collection of negative charge suppresses the positive potential within the anode. The electrons, consequently, will be repelled in the radial direction by the negative electrostatic force imparted on them by their fellow electrons as they converge on the center of the device. By conservation of energy, the electrons will be repelled at a radius r_c at which the potential is equal to that of the cathode grid. Thus, one boundary condition for this system is

$$V(r_c) = V_c \quad (1)$$

where r_c is the radius of a virtual cathode, and V_c is the voltage of the real cathode grid. It may be argued that since the virtual cathode is 100% transparent, then the flow of electrons from the virtual cathode is space charge limited. Thus, another condition that may be applied at r_c is

$$\frac{\partial V(r_c)}{\partial r} = 0. \quad (2)$$

If the electrons are born in UCA SIECs through volume ionization along with grid emission, then a spread in the energy of the particles will develop. If we still require that the electrons have no angular velocity, we can observe what effect the spread in the radial energy of electrons will have on the boundary condition at r_c . Since some electrons will be born with energy $-eV_a \leq -eV < -eV_c$, they will be repelled at a radius $r_c < r \leq R_a$, where R_a is the radius of the anode, and r corresponds to the radius within the anode at which the potential is V . Thus, fewer electrons will exist at r_c in this case than in the previous case. Fewer electrons means the electrostatic force is not as great at r_c , and the electrons will converge to a new radius $0 < r_{c1} < r_c$, at which point they are repelled back through the anode. Thus, the boundary condition of (1) now becomes the following boundary condition:

$$V(r_{c1}) = V_c. \quad (3)$$

The radius of the new virtual cathode r_{c1} will approach zero and (3) will always hold for this case, as long as some electrons born at the real cathode radius are included in the energy distribution. If electrons born at the real cathode are not included in the electron energy distribution, then

$$V(r_{c1}) = V_{\min} \quad (4)$$

where V_{\min} represents the birth potential of the highest energy group of electrons in the distribution. In addition, since the virtual cathode is 100% transparent, we obtain

$$\frac{\partial V(r_{c1})}{\partial r} = 0 \quad (5)$$

and in the limiting case, as $r_c \rightarrow 0$, we obtain

$$V(0) = V_{\min} \quad (6)$$

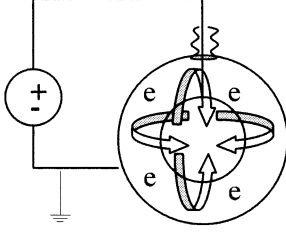
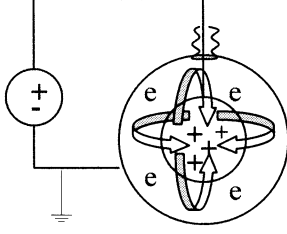
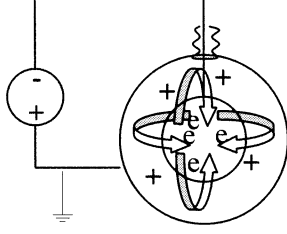
$$\frac{\partial V(0)}{\partial r} = 0. \quad (7)$$

Finally, we wish to analyze the affect of electrons with an angular velocity distribution, on the boundary conditions, while assuming that the sum of angular energy and radial energy is the same for all electrons. A spread in angular velocity will have a similar affect as a spread in radial velocity, in that the radius of the virtual cathode will be reduced. Once again, the radius of the new virtual cathode r_{c1} will approach zero as the spread in angular energy increases, and (3) will apply, as long as some electrons with zero angular velocity are included in the distribution. If no electrons with zero angular energy are included in the distribution, then the condition in (4) will apply, where V_{\min} corresponds to the birth potential of the group of electrons with the least angular energy, or largest radial energy. In addition, the boundary condition in (5) still applies, and (6) and (7) apply as $r_{c1} \rightarrow 0$. In theory, (3) will hold as long as some portion of the electrons has zero angular energy, because the electrons will converge head on at the center, and repel each other. In practice, however, these electrons will not meet directly head on, but will pass by each other at the center with a minimum velocity, and then be re-accelerated toward the opposite side of the anode grid, from which they entered [28]. Thus, (3) will not generally hold for a practical system, as electrons born at a potential of $V_c \leq V < V_{\min}$, within the inter-electrode space, will not be repelled within the anode space, and (4) will apply. As $r_{c1} \rightarrow 0$, (6) and (7) will apply. Similar arguments can be made to derive the boundary conditions of a UAC SIEC.

Next, we wish to consider bipolar SIECs, in particular, we derive the boundary conditions for the BAC SIEC. First we will derive the boundary conditions for the case of mono-energetic particles with no angular energy. If we initially ignore the electrons, the circulating ions will form a virtual anode at r_a . If we now consider electrons existing within the cathode of a BAC SIEC, then these electrons will have a screening affect that reduces the amount of electrostatic repulsion that ions feel from their fellow ions as they converge at r_a . Since the electrostatic repulsion is reduced, the virtual anode at r_a , formed by converging ions will form closer to the center, $0 \leq r_{a1} < r_a$, as indicated by Hirsch [13]. Thus, we will obtain the boundary condition in (3) if we replace r_{c1} by r_{a1} and the cathode voltage, V_c with the anode voltage V_a . Electrons emitted by the cathode will be accelerated through virtual anode, and converge at the center until the electrostatic force of the converging electrons causes the electrons to repel each other, at a radius, r_{c1} , forming a virtual cathode, at which (3) will apply. Some ions from the virtual anode at r_{a1} , will be accelerated through the virtual cathode and form a second virtual anode at r_{a2} . An infinite number of alternating virtual electrodes will form in this way.

It is assumed that the particle currents are space charge limited at the virtual electrodes, since the electrodes have a transparency of $\eta = 100\%$, thus, if we consider the first virtual anode, we can apply (5), if we replace r_{c1} with r_{a1} . This condition also applies to the rest of the virtual electrodes within the device. If a spread in the radial energy distribution of ions develops due to volume ionization in the inter-electrode space, then, analogous to the unipolar systems, the radius of the first virtual anode at $r = r_{a1}$ will shrink to $r = r'_{a1}$, where, $0 < r'_{a1} < r_{a1}$. In this case, we can apply (3) and (5) if r_{c1} is re-

TABLE I
THIS TABLE IDENTIFIES DIFFERENT TYPES OF INERTIAL ELECTROSTATIC DEVICES ANALYZED IN THIS WORK

Designation	Uni-polar Cathode-Anode System (UCA)	Bi-polar Cathode-Anode System (BCA)	Bi-polar Anode-Cathode System (BAC)
Schematic			
Primary Particle	electron	electron	ion
Secondary Particle	-----	ion	electron
Boundary Conditions			
Anode Grid $\eta < 1.0$	$V(R_a) = V_a,$ $0 < R_a < R_c$	$V(R_a) = V_a,$ $0 < R_a < R_c$	$V(R_a) = V_a,$ $0 < R_c < R_a$
Cathode Grid $\eta < 1.0$	$V(R_c) = V_c,$ $0 < R_a < R_c$	$V(R_c) = V_c,$ $0 < R_a < R_c$	$V(R_c) = V_c,$ $0 < R_c < R_a$
Virtual Electrodes $\eta = 1.0$			
For mono-energetic distribution	$V(r_c) = V_c$ $\partial V(r_c)/\partial r = 0$ $0 < r_c < R_a$	$V(r_{ci,ai}) = V_{c,a}$ $\partial V(r_{ci,ai})/\partial r = 0$ $0 < r_{ai} < r_{ci} < R_a$	$\partial V(r_{ai,ci})/\partial r = 0$ $V(r_{ai,ci}) = V_{a,c}$ $0 < r_{ci} < r_{ai} < R_c$
For radial energy distribution	$V(r_{c1}) = V_c$ $\partial V(r_{c1})/\partial r = 0$ $0 < r_{c1} < r_c < R_a$	$V(r_{ci,ai}) = V_{c,a}$ $\partial V(r_{ci,ai})/\partial r = 0$ $0 < r_{ai} < r_{ci} < R_a$	$V(r_{ai,ci}) = V_{a,c}$ $\partial V(r_{ai,ci})/\partial r = 0$ $0 < r_{ci} < r_{ai} < R_c$
For angular energy distribution	$V(0) = V_{\min},$ $V_c \leq V_{\min} < V_a$ $\partial V(0)/\partial r = 0$	$V(0) = V_{\min},$ $V_c \leq V_{\min} < V_a$ $\partial V(0)/\partial r = 0$	$V(0) = V_{\max},$ $V_c \leq V_{\max} < V_a$ $\partial V(0)/\partial r = 0$

placed by r'_{a1} and the cathode potential, V_c , is replaced by the anode potential V_a . Similarly, the radii of subsequent virtual electrodes are also reduced. If a spread in the angular energy of the ions is now considered, we can deduce from our analysis of unipolar systems that increasing the spread in angular energy results in shrinking the radii of the virtual electrodes. In addition, we assume that two ions with zero angular energy, converging at the center, do not collide head on. Instead, they will pass by each other with a minimum velocity [28]. Thus, a V_{\max} exists where ions with small angular energy, or a radial energy greater than eV_{\max} will circulate the entire diameter of the cathode. In this case, (4) is the appropriate condition with V_{\min} replaced by V_{\max} . Finally, we will obtain the condition in (7), as the radii of the virtual electrodes shrink to zero.

UCA, BCA, and BAC SIECs are summarized in Table I with their schematics given in Figs. 3–5, respectively. In this table, the primary particle refers to the injected particle, which is the electron for UCA and BCA systems, and the ion for the BAC systems. The secondary particle is the particle assumed to be confined within the inner grid of the system. Also, it should be mentioned that, in Table I, the subscripts ci and ai refer to i th virtual cathode or virtual anode for the infinite virtual electrode structure that exists in the bipolar SIECs under ideal conditions.

E. Purpose, Scope of Work

Collisionless models of UCA, BCA, and BAC SIECs, given in Table I, will be derived based on previous analytical work performed by Langmuir and Blodgett [18], Hirsch [13], Dolan [20],

[29], Swanson [21], [30], and Lavrent'ev [19], in Section II. A new and efficient method for evaluating the resulting integral equations will then be presented. In Section III, the method is validated by computing solutions for the UCA system, which may be compared to solutions calculated by Swanson [30]. In addition, the method is benchmarked against Hirsch's solutions by considering mono-energetic particle distributions. A parametric study of the UCA, BCA, and BAC SIECs is performed, and conditions most conducive to a double potential well structure are delineated. A discussion regarding the reliability of the method, and how the results of the parametric study for the BAC SIEC relate to the experimental work of Gu [17] and recent computations by Miley [26], will be provided in Section IV. While more collisional models, such as Ohnishi *et al.* [27], are needed to accurately model experimental SIECs, the extensive parametric study made possible by the collisionless model presented here can serve as a valuable benchmark for studying trends in IEC behavior.

II. DERIVATION OF MODEL, METHOD OF SOLUTION

A. Derivation of Collisionless Models

Neglecting collisions of any kind, analysis of the UCA may be conducted by solving Poisson's equation, while simultaneously applying the conditions of conservation of energy and current continuity. Langmuir and Blodgett assumed that electrons were mono-energetic, emitted with zero kinetic energy, and never have a velocity component in the angular direction. Poisson's equation for this situation is

$$\frac{1}{r^2} \frac{d}{dr} \left(r^2 \frac{dV}{dr} \right) = \frac{\rho_e}{\varepsilon_o} \quad (8)$$

where V is the voltage at a radius r measured with respect to the cathode, which is assumed to be at ground potential, and ρ_e is the charge distribution due to the electrons. The electron current I_e is related to the charge distribution at a radius r by

$$I_e = 4\pi r^2 \rho_e v. \quad (9)$$

In this equation, v is the velocity of the electrons at r . If we let m_e denote the mass of an electron, and e denote the absolute magnitude of the electron charge, then applying conservation of energy to the electrons emitted from the inner surface of the cathode, we can relate the velocity of the electrons at r to the potential at r with

$$\frac{1}{2} m_e v^2 = Ve. \quad (10)$$

Substituting (9) and (10) into (8), we arrive at

$$\frac{1}{r^2} \frac{d}{dr} \left(r^2 \frac{dV}{dr} \right) = \frac{I_e}{4\pi\varepsilon_o} \left(\frac{m_e}{2e} \right)^{1/2} \frac{1}{r^2 V^{1/2}}. \quad (11)$$

A typical solution computed from (11), is provided in Fig. 1. In Fig. 1, the potential and radius of the anode have been normalized to unity, while the cathode is assumed to be at ground potential.

Hirsch followed the analysis of Langmuir and Blodgett by assuming that ions and electrons are emitted from their respective surfaces with zero kinetic energy, so that they are mono-energetic, with no component of their energy in the angular direction. For this situation, Poisson's equation takes the form given by

$$\frac{1}{r^2} \frac{d}{dr} \left(r^2 \frac{dV}{dr} \right) = \frac{1}{\varepsilon_o} (\rho_e - \rho_i) \quad (12)$$

where ρ_e and ρ_i are the electron and ion charge distributions, respectively, and ε_o is the permittivity of free space. We can represent the electron current I_e and ion current I_i separately, by

$$I_e = 4\pi r^2 \rho_e v_e \quad (13)$$

and

$$I_i = 4\pi r^2 \rho_i v_i \quad (14)$$

for electrons with velocity v_e , and ions with velocity, v_i . Parallel with the analysis performed by Langmuir and Blodgett, the electron and ion velocities at a radius, r , are related to the potential at r by independently applying the conservation of energy principle to electrons and ions

$$\frac{1}{2} m_e v_e^2 = e(V - V_c) \quad (15)$$

$$\frac{1}{2} m_i v_i^2 = |eV|. \quad (16)$$

In (15), V_c represents the cathode potential, and m_i represents the ion mass in (16). Substituting (15) and (16) into (13) and (14), respectively, and substituting (13) and (14) into (12), we obtain

$$\begin{aligned} & \frac{1}{r^2} \frac{d}{dr} \left(r^2 \frac{dV}{dr} \right) \\ &= \frac{I_e}{4\pi\varepsilon_o} \left(\frac{m_e}{2e} \right)^{1/2} \frac{1}{r^2 (V - V_c)^{1/2}} \\ & - \frac{I_i}{4\pi\varepsilon_o} \left(\frac{m_i}{2e} \right)^{1/2} \frac{1}{r^2 V^{1/2}}. \end{aligned} \quad (17)$$

In order to solve for the potential, and generalize the solutions, (17) is parameterized by substituting

$$Y = -\frac{V}{V_c} \quad \text{and} \quad X = \frac{r}{R_c} \quad (18)$$

where R_c is the cathode radius, and $-V_c$ is the cathode potential

$$\frac{1}{X^2} \frac{d}{dX} X^2 \frac{dY}{dX} = \frac{K_i}{X^2} [Y^{-1/2} - \lambda_i (1 - Y)^{-1/2}] \quad (19)$$

and K_i and λ_i are given by

$$K_i = \frac{I_i}{V_c^{3/2}} \left(\frac{m_i}{2e} \right)^{1/2} \frac{1}{4\pi\varepsilon_o} \quad (20)$$

and

$$\lambda_i = \frac{I_e}{I_i} \left(\frac{m_e}{m_i} \right)^{1/2}. \quad (21)$$

Recalling from Section I that mono-energetic particle distributions in BAC devices generate an infinite number of potential wells, Hirsch applied

$$Y(r_{a1}) = 0 \quad (22)$$

and

$$\frac{\partial Y(r_{a1})}{\partial r} = 0 \quad (23)$$

at the boundary of the first virtual anode, where the real anode grid is at ground potential. Hirsch was able to determine the ratio of the radius of the real cathode to the radius of the first virtual anode by inspecting the radius at which the solution to (19) crossed the $Y = 1$ axis (the normalized cathode grid potential). To compute solutions between the first virtual anode at the radius r_{a1} and the first virtual cathode at r_{c1} , Hirsch replaced K_i and λ_i in (19) with K_e and λ_e , respectively, where K_e and λ_e are given by

$$K_e = K_i \lambda_i \quad (24)$$

and

$$\lambda_e = (\lambda_i)^{-1}. \quad (25)$$

The solution to (19) between the first virtual anode and the first virtual cathode can be obtained by once again utilizing (22) and (23). Theoretically, an infinite number of virtual electrodes may be computed in this way. A solution to (19) is provided in Fig. 2, where the cathode radius and potential are normalized to unity.

Hirsch's mono-energetic model does not account for spreads in the total and angular energies of the particles. However, Dolan [20], [29], Swanson [21], [30], and Lavrent'ev, [19] created more realistic models that included spreads in the total and angular energies of particles. They modeled the UCA system and a BCA SIEC configuration. Analysis of the BCA SIEC includes solving the form of Poisson's equation, in (12), and then using the following forms of electron and ion currents

$$I_e = 4\pi r^2 \rho_e v_{e,r} \quad (26)$$

and

$$I_i = 4\pi r^2 \rho_i v_{i,r} \quad (27)$$

where $v_{e,r}$ and $v_{i,r}$ are the electron and ion radial velocities, respectively. Expressions for the electron and ion radial velocities can be obtained by separately applying the conservation of energy principle to the electrons and ions. If it is assumed that electrons are allowed to enter the system with total energy eW_e , where $0 \leq eW_e \leq eV_a$ then the energy relationship for electrons is given by

$$-eW_e = \frac{1}{2}m_e v_{r,e}^2 + \frac{1}{2}m_e v_{\phi,e}^2 - eV. \quad (28)$$

To explain the limits imposed on eW_e , consider an electron at r , within the anode. If an electron is introduced at the surface of the anode grid with zero kinetic energy, then the total energy of the electron will be $-eW_e = -eV_a$. At the anode surface, the electrons will not experience any acceleration, because it is at the point of maximum potential. Thus, an electron introduced at this point must have a minimum kinetic energy of $e(V_a - V)$

to reach r . The minimum limit of the total electron energy at r is thus, $-eW_e = -eV_a + e(V_a - V) = -eV$. Electrons introduced at the cathode of a BCA system will have a total kinetic energy of $-eW_e = 0$, and will be accelerated toward a radius r within the anode. An electron introduced at the cathode of the BCA system with any kinetic energy will be able to escape from the system. Thus, the limits of integration for the total electron energy are, $-eV \leq -eW_e \leq 0$.

The energy relationship for ions is given by

$$eW_i = \frac{1}{2}m_i v_{r,i}^2 + \frac{1}{2}m_i v_{\phi,i}^2 + eV. \quad (29)$$

In this equation, $v_{\phi,i}$ is the angular velocity of the ions. In (29), it is assumed that ions are introduced with energy eW_i . The limits imposed on the ion energy may be determined by assuming an ion is introduced to the BCA system at a radius r within the anode, where the voltage is V . At this point, the ion will have energy, $eW_i = eV$. If the ion is introduced at this point with a kinetic energy $e(V_a - V)$, then the total energy of the ion at this point will be $eW_i = eV + e(V_a - V) = eV_a$. An ion introduced with greater kinetic energy will escape to the cathode. Thus, the limits imposed on the total energy that an ion may be introduced to the BCA system are, $eV \leq eW_i \leq eV_a$.

Since collisions are neglected, the angular momentum of electrons and ions are conserved, in addition to the total energy of electrons and ions. The angular momentum of electrons and of ions is defined

$$L_e = m_e v_{\phi,e} r \quad (30)$$

$$L_i = m_i v_{\phi,i} r. \quad (31)$$

From (30) and (31), we can define the angular energies of electrons and ions as

$$eS_e = \frac{L_e^2}{2m_e R_a^2} = \frac{1}{2}m_e v_{\phi,e}^2 \left(\frac{r^2}{R_a^2} \right) \quad (32)$$

and

$$eS_i = \frac{L_i^2}{2m_i R_a^2} = \frac{1}{2}m_i v_{\phi,i}^2 \left(\frac{r^2}{R_a^2} \right). \quad (33)$$

We can relate the radial velocity of the electrons to the potential, total energy of the electrons, and angular energy of the electrons with (28) and (32)

$$v_{r,e} = \left(\frac{2e}{m_e} \right)^{1/2} \left(V - W_e - S_e \frac{R_a^2}{r^2} \right)^{1/2}. \quad (34)$$

A similar expression can be constructed for the ions, using (29) and (33)

$$v_{r,i} = \left(\frac{2e}{m_i} \right)^{1/2} \left(W_i - V - S_i \frac{R_a^2}{r^2} \right)^{1/2}. \quad (35)$$

Relations in (34) and (35) allow us to determine the limits that should be imposed on the angular energy of the electrons and the ions. These particles can have angular energy ranging from zero up to a maximum corresponding to the condition that all of the particles' energy is in a direction perpendicular to the radial

direction [29]. For electrons, this maximum energy corresponds $v_{r,e} = 0$. Inserting this into (34), we see that the maximum angular energy is

$$S_{e,\max} = \left(\frac{r^2}{R_a^2} \right) (V - W_e). \quad (36)$$

A similar relationship can be developed for the maximum angular ion energy

$$S_{i,\max} = \left(\frac{r^2}{R_a^2} \right) (W_i - V). \quad (37)$$

Solving (26) and (27) for the charge densities and plugging (34) and (35) in for the radial electron and ion velocities, we obtain

$$\rho_e(S_e, W_e) = \frac{I_e(S_e, W_e)}{4\pi r^2} \left(\frac{m_e}{2e} \right)^{1/2} \frac{1}{\left(V - W_e - S_e \frac{R_a^2}{r^2} \right)^{1/2}} \quad (38)$$

and

$$\rho_i(S_i, W_i) = \frac{I_i(S_i, W_i)}{4\pi r^2} \left(\frac{m_i}{2e} \right)^{1/2} \frac{1}{\left(W_i - V - S_i \frac{R_a^2}{r^2} \right)^{1/2}}. \quad (39)$$

Thus, the total electron and ion charge densities are computed with the following:

$$\rho_e = \int_0^V dW_e \int_0^{\left(\frac{r^2}{R_a^2} \right)(V-W_e)} dS_e \rho_e(S_e, W_e) \quad (40)$$

$$\rho_i = \int_V^{V_a} dW_i \int_0^{\left(\frac{r^2}{R_a^2} \right)(W_i-V)} dS_i \rho_i(S_i, W_i). \quad (41)$$

(40) and (41) can be inserted into the form of Poisson's equations, in (12) to get the following expression, for the BCA system:

$$\frac{1}{r^2} \frac{d}{dr} \left(r^2 \frac{dV}{dr} \right) = f_e(r, V) - g_i(r, V). \quad (42)$$

In this equation, $f_e(r, V)$ and $g_i(r, V)$ are represented with

$$f_e(r, V) = \frac{1}{4\pi\epsilon_0 r^2} \left(\frac{m_e}{2e} \right)^{1/2} \times \int_0^V dW_e \int_0^{\left(\frac{r^2}{R_a^2} \right)(V-W_e)} dS_e \frac{I_e(S_e, W_e)}{\left(V - W_e - S_e \frac{R_a^2}{r^2} \right)^{1/2}} \quad (43)$$

and

$$g_i(r, V) = \frac{1}{4\pi\epsilon_0 r^2} \left(\frac{m_i}{2e} \right)^{1/2} \times \int_V^{V_a} dW_i \int_0^{\left(\frac{r^2}{R_a^2} \right)(W_i-V)} dS_i \frac{I_i(S_i, W_i)}{\left(W_i - V - S_i \frac{R_a^2}{r^2} \right)^{1/2}}. \quad (44)$$

A similar expression can be derived for the UCA system simply by deleting the term for ions, thus obtaining

$$\frac{1}{r^2} \frac{d}{dr} \left(r^2 \frac{dV}{dr} \right) = f_e(r, V). \quad (45)$$

(42) and (45) are normalized in order to simplify and generalize the solutions for the UCA and BCA systems, respectively. These equations are generalized by substituting

$$\begin{aligned} X &= \frac{r}{R_a} \\ Y &= \frac{V}{V_a} \\ Y_{e,E} &= \frac{W_e}{V_a} \\ Y_{i,E} &= \frac{S_i}{V_a} \\ Y_{e,\phi} &= \frac{W_e}{V_a} \end{aligned}$$

and

$$Y_{i,\phi} = \frac{W_i}{V_a} \quad (46)$$

into (42) and (45) to obtain the following expressions for the UCA system and the BCA system, respectively:

$$\frac{1}{X^2} \frac{d}{dX} \left(X^2 \frac{dY}{dX} \right) = F_e(X, Y) \quad (47)$$

$$\frac{1}{X^2} \frac{d}{dX} \left(X^2 \frac{dY}{dX} \right) = F_e(X, Y) - G_i(X, Y) \quad (48)$$

where $F_e(X, Y)$ and $G_i(X, Y)$ are given as

$$\begin{aligned} F_e(X, Y) &= \frac{V_a}{4\pi\epsilon_0 \left(\frac{2eV_a}{m_e} \right)^{1/2}} \cdot \int_0^Y dY_{e,E} \\ &\times \int_0^{X^2(Y-Y_{e,E})} dY_{e,\phi} \frac{I_e(Y_{e,E}, Y_{e,\phi})}{X^2[Y - Y_{e,E} - (Y_{e,\phi}/X^2)]^{1/2}} \end{aligned} \quad (49)$$

and

$$\begin{aligned} G_i(X, Y) &= \frac{V_a}{4\pi\epsilon_0 \left(\frac{2eV_a}{m_i} \right)^{1/2}} \cdot \int_Y^1 dY_{i,E} \\ &\times \int_0^{X^2(Y_{i,E}-Y)} dY_{i,\phi} \frac{I_i(Y_{i,E}, Y_{i,\phi})}{X^2[Y_{i,E} - Y - (Y_{i,\phi}/X^2)]^{1/2}}. \end{aligned} \quad (50)$$

The normalized total and angular electron energies are represented by $Y_{e,E}$ and $Y_{e,\phi}$, while the normalized total and angular ion energy is represented by $Y_{i,E}$ and $Y_{i,\phi}$. Equations (47) and

(48) were solved while applying the following boundary conditions:

$$Y(1) = 0 \quad (51)$$

$$\frac{dY(0)}{dX} = 0. \quad (52)$$

The model for the BAC system can be derived in much the same way as the BCA system. Again, (12) is solved, using the expressions for electron and ion current in (26) and (27). Then, the conservation of energy laws in (28) and (29) are applied to the electrons and ions, respectively. Expressions for the electron angular momentum and the ion angular momentum are provided in (30) and (31), while relationships are developed for the electron and ion angular energies in (32) and (33). Expressions for the radial velocities of electrons and ions are provided in (34) and (35), to be plugged into the equations for the electron and ion current, (26) and (27). Finally, maximum angular energies of the electrons and ions are solved for and provided by (36) and (37).

Analysis of the BAC system deviates from that of the BCA system because the potential of the inner electrode is now $-V_c$. Also, the limits on the total energy of the electrons W_e and ions, W_i , for the BAC system, are different than the limits for the BCA system. Consider an ion that is introduced to the BAC system on the inner surface of the cathode. If the ion is born with zero kinetic energy, then the total energy of the ion at this point will be $eW_i = -eV_c$. However, for this ion to travel to a radius r within the cathode, it must be introduced with a minimum kinetic energy of $e(V + V_c)$. Thus, the minimum total energy of an ion at a radius r , within the cathode, is $eW_i = -eV_c + e(V + V_c) = eV$. Ions born at the anode will have a total energy of $eW_i = 0$. Ions born with kinetic energy at this point will be able to escape from the system. Thus, the limits imposed on the ion energy within the cathode of a BAC system, at a radius r , are $eV \leq eW_i \leq 0$.

The limits imposed on the total energy of the electrons is determined if we consider an electron born at a radius r inside of the cathode. If the electron is introduced with zero kinetic energy, then the electron will have a total energy $-eW_e = -eV$. An electron introduced at this point with a kinetic energy of $e(V_c + V)$ will have a total energy of $-eW_e = e(V_c + V) - eV = eV_c$. Thus, the limits imposed on the total energy of the electron in the BAC device are $-eV \leq -eW_e \leq eV_c$, noting that the cathode voltage is defined as $-V_c$.

Thus, using expressions in (38) and (39), we are able to arrive at the following relations for the electron and ion charge densities at a radius r :

$$\rho_e = \int_{-V_c}^V dW_e \int_0^{(\frac{r^2}{R_a^2})(V-W_e)} dS_e \rho_e(S_e, W_e) \quad (53)$$

$$\rho_i = \int_V^0 dW_i \int_0^{(\frac{r^2}{R_a^2})(W_i-V)} dS_i \rho_i(S_i, W_i). \quad (54)$$

Plugging (53) and (54) into (12), we arrive at the following BAC model

$$\frac{1}{r^2} \frac{d}{dr} \left(r^2 \frac{dV}{dr} \right) = g_e(r, V) - f_i(r, V) \quad (55)$$

where $g_e(r, V)$ and $f_i(r, V)$ are represented by

$$g_e(r, V) = \frac{1}{4\pi\epsilon_0 r^2} \left(\frac{m_i}{2e} \right)^{1/2} \times \int_{-V_c}^V dW_i \int_0^{(\frac{r^2}{R_a^2})(W_i-V)} dS_i \frac{I_i(S_i, W_i)}{\left(W_i - V - S_i \frac{R_a^2}{r^2} \right)^{1/2}} \quad (56)$$

and

$$f_i(r, V) = \frac{1}{4\pi\epsilon_0 r^2} \left(\frac{m_e}{2e} \right)^{1/2} \times \int_V^0 dW_e \int_0^{(\frac{r^2}{R_a^2})(V-W_e)} dS_e \frac{I_e(S_e, W_e)}{\left(V - W_e - S_e \frac{R_a^2}{r^2} \right)^{1/2}} \quad (57)$$

(55) is normalized to aid in solving the equation and generalizes the solutions, by substituting (18) and (46) into (55) to arrive at

$$\frac{1}{X^2} \frac{d}{dX} \left(X^2 \frac{dY}{dX} \right) = F_i(X, Y) - G_e(X, Y). \quad (58)$$

In (58), $F_i(X, Y)$ and $G_e(X, Y)$ are, respectively

$$F_i(X, Y) = \frac{V_a}{4\pi\epsilon_0 \left(\frac{2eV_a}{m_e} \right)^{1/2}} \cdot \int_0^Y dY_{i,E} \times \int_0^{X^2(Y-Y_{i,E})} dY_{i,\phi} \frac{I_i(Y_{i,E}, Y_{i,\phi})}{X^2[Y - Y_{i,E} - (Y_{i,\phi}/X^2)]^{1/2}} \quad (59)$$

$$G_e(X, Y) = \frac{V_a}{4\pi\epsilon_0 \left(\frac{2eV_a}{m_i} \right)^{1/2}} \cdot \int_Y^1 dY_{e,E} \times \int_0^{X^2(Y_{e,E}-Y)} dY_{e,\phi} \frac{I_e(Y_{e,E}, Y_{e,\phi})}{X^2[Y_{e,E} - Y - (Y_{e,\phi}/X^2)]^{1/2}}. \quad (60)$$

B. Assumption of Current Distribution

For the systems in Table I, the models we have derived are given by (47) for the UCA system and by (48), and (58) for BCA and BAC systems. Swanson [21] computed solutions for the BCA system assuming that the electron and ion currents have rectangular or Gaussian distributions with respect to $Y_{e,\phi}$ and $Y_{e,E}$ for electrons, and $Y_{i,\phi}$ and $Y_{i,E}$ for ions. Here we will

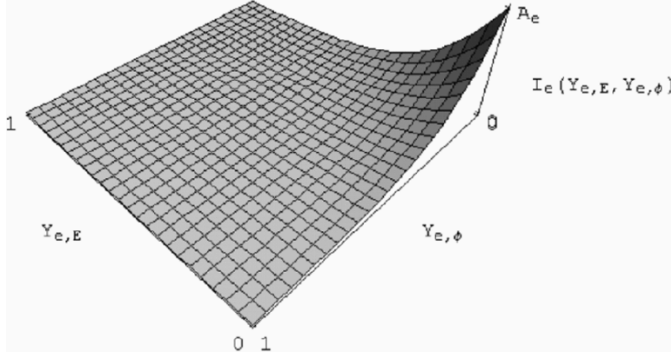


Fig. 6. Gaussian electron current distribution over the $Y_{e,E}, Y_{e,\phi}$ plane, for BCA systems. Gaussian ion current distribution over the $Y_{i,E}, Y_{i,\phi}$ plane for BAC systems.

proceed in a similar manner by assuming that the electron and ion currents have Gaussian distributions with respect to the parameters just mentioned. Thus, the electron current may be represented by

$$I_e(Y_{e,E}, Y_{e,\phi}) = A_e e^{-(Y_{e,E}/\sigma_{e,E})^2} e^{-(Y_{e,\phi}/\sigma_{e,\phi})^2} \quad (61)$$

with $\sigma_{e,E}$ and $\sigma_{e,\phi}$ representing the spreads in the normalized total and angular electron energy, and where the constant A_e is computed by recognizing that the circulating electron current for the BCA system is

$$I_{ce} = V_a^2 \int_0^1 dY_{e,E} \int_0^{1-Y_{e,E}} dY_{e,\phi} I_e(Y_{e,E}, Y_{e,\phi}). \quad (62)$$

As electrons converge on the center of the anode of a BCA SIEC, they will either repel each other back through the anode grid (of transparency η) in the radial direction, or they will traverse diametrically through the inner anode space and pass through the opposite side of the anode grid from which they entered. The current generated by electrons making several passes back and forth through the anode grid, before being collected by the grid, is known as the circulating electron current. Dolan [29] showed that the circulating current of a particle is related to the grid current of that particle by the following relationship:

$$I_{ce} = I_{ge} \frac{2\eta}{(1-\eta^2)} \quad (63)$$

where I_{ce} is the circulating electron current and I_{ge} is the grid electron current. An analogous expression exists for the circulating ions, where I_{ci} is the circulating ion current and I_{gi} is the grid ion current.

For the BCA configuration, the grid electron current is distributed over the normalized electron total and angular energies, $Y_{e,E}$ and $Y_{e,\phi}$, as shown in Fig. 6. One, thus, has for A_e [21], [30]

$$A_e = [I_{ce} / (V_a^2 \sigma_{e,\phi} \sigma_{e,E})] \cdot \left\{ 1 - e^{-(1/\sigma_{e,E})^2} - [\sigma_{e,\phi} / (\sigma_{e,\phi} - \sigma_{e,E})] \cdot [e^{-(1/\sigma_{e,\phi})^2} - e^{-(1/\sigma_{e,E})^2}] \right\}^{-1}. \quad (64)$$

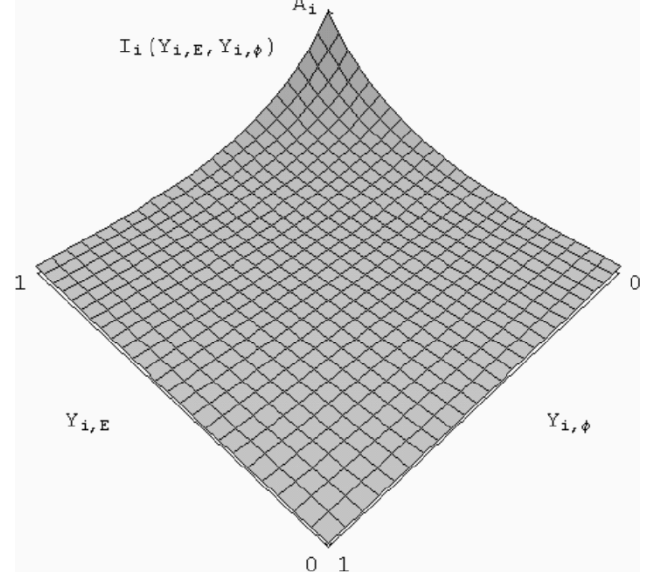


Fig. 7. Gaussian ion current distribution over the $Y_{i,E}, Y_{i,\phi}$ plane for BCA systems. Gaussian electron current distribution over the $Y_{e,E}, Y_{e,\phi}$ plane for BAC systems.

Substituting (61)–(64) into (49), for the BCA system, we obtain the following expression:

$$F_e(X, Y) = \frac{K_e}{X^2} \int_0^Y dY_{e,E} \times \int_0^{X^2(Y-Y_{e,E})} dY_{e,\phi} \frac{e^{-(Y_{e,E}/\sigma_{e,E})^2} e^{-(Y_{e,\phi}/\sigma_{e,\phi})^2}}{[Y - Y_{e,E} - (Y_{e,\phi}/X^2)]^{1/2}} \quad (65)$$

where K_e is defined by

$$K_e = [2\eta / (1 - \eta^2)] \cdot \left\{ [1 / (4\pi\epsilon_0 \sigma_{e,E} \sigma_{e,\phi})] \cdot [m_e / (2e)]^{1/2} \right\} \cdot \left\{ 1 - e^{-(1/\sigma_{e,E})^2} - [\sigma_{e,\phi} / (\sigma_{e,\phi} - \sigma_{e,E})] \cdot [e^{-(1/\sigma_{e,\phi})^2} - e^{-(1/\sigma_{e,E})^2}] \right\}^{-1} \cdot (I_{ce} / V_a^{3/2}). \quad (66)$$

The ion current, for the BCA configuration, is distributed over $Y_{i,E}$ and $Y_{i,\phi}$, as shown in Fig. 7, where $Y_{i,E}$ and $Y_{i,\phi}$ are the normalized ion total and angular energies, respectively.

The expression for the ion current is given by

$$I_i(Y_{i,E}, Y_{i,\phi}) = A_i e^{[(Y_{i,E}-1)/\sigma_{i,E}]^2} e^{-(Y_{i,\phi}/\sigma_{i,\phi})^2} \quad (67)$$

where $\sigma_{i,E}$ and $\sigma_{i,\phi}$ represent the spreads in the normalized total and angular ion energy, and the value of the constant A_i is computed by recognizing that the circulating ion current, for the BCA system is given by

$$I_{ci} = V_a^2 \int_{Y_{\min}}^1 dY_{i,E} \int_0^{Y_{i,E}-Y_{\min}} dY_{i,\phi} I_i(Y_{i,E}, Y_{i,\phi}). \quad (68)$$

Evaluating A_i is not as straightforward as the evaluation of A_e because the electron is allowed to have $0 \leq Y_{e,\phi} \leq 1 - Y_{e,E}$ and $0 \leq Y_{e,E} \leq 1$. The ion has energies in the range $0 \leq Y_{i,\phi} \leq$

$(Y_{i,E} - Y_{\min})$ and $Y_{\min} \leq Y_{i,E} \leq 1$. These limits depend on the minimum normalized potential within the anode, Y_{\min} , which is information that we seek from the solution of (51). Solving for A_i , as a function of Y_{\min} , yields

$$A_i(Y_{\min}) = [I_{ci} / (V_a^2 \sigma_{i,\phi} \sigma_{i,E})] \cdot \left\{ 1 - e^{((Y_{\min}-1)/\sigma_{i,E})} + [\sigma_{i,\phi} / (\sigma_{i,\phi} - \sigma_{i,E})] \cdot \left[e^{((Y_{\min}-1)/\sigma_{i,\phi})} - e^{((Y_{\min}-1)/\sigma_{i,E})} \right] \right\}^{-1} \quad (69)$$

Using an initial guess of $Y_{\min,0} = 0$, we can generate an approximate solution to (48). The minimum potential of this solution is denoted as $Y_{\min,1}$. $Y_{\min,1}$ can be inserted into (69) to generate another approximate solution to (48). This iteration can be repeated until the difference between successive computations, $A_i(Y_{\min})^i$ and $A_i(Y_{\min})^{i+1}$, is less than some specified tolerance.

Equations (67)–(69) are substituted into (50) to obtain the following expression:

$$G_i(X, Y) = \frac{K_i}{X^2} \int_Y^1 dY_{i,E} \times \int_0^{X^2(Y_{i,E}-Y)} dY_{i,\phi} \frac{e^{-(Y_{i,E}/\sigma_{i,E})} e^{-(Y_{i,\phi}/\sigma_{i,\phi})}}{[Y_{i,E} - Y - (Y_{i,\phi}/X^2)]^{1/2}} \quad (70)$$

where the form of K_i is provided as

$$K_i = [2\eta/(1 - \eta^2)] \cdot \{ [1/(4\pi\epsilon_0 \sigma_{i,E} \sigma_{i,\phi})] \cdot [m_i/(2e)]^{1/2} \} \cdot \left\{ 1 - e^{((Y_{\min}-1)/\sigma_{i,E})} + [\sigma_{i,\phi} / (\sigma_{i,\phi} - \sigma_{i,E})] \cdot \left[e^{((Y_{\min}-1)/\sigma_{i,\phi})} - e^{((Y_{\min}-1)/\sigma_{i,E})} \right] \right\}^{-1} \cdot (I_i/V_a^{3/2}). \quad (71)$$

Equation (65) may be substituted into (47) and (48), while (70) may be substituted back into (48) to obtain solutions for the UCA and BCA configurations, respectively.

For the BAC system, represented by (58), the distribution of ion current is now represented with Fig. 6, and the distribution of electron current is now illustrated in Fig. 7. The ion current is represented with

$$I_i(Y_{i,E}, Y_{i,\phi}) = A_i e^{-(Y_{i,E}/\sigma_{i,E})} e^{-(Y_{i,\phi}/\sigma_{i,\phi})} \quad (72)$$

and the circulating ion current is now defined with

$$I_{ci} = V_c^2 \int_0^1 dY_{i,E} \int_0^{1-Y_{i,E}} dY_{i,\phi} I_i(Y_{i,E}, Y_{i,\phi}). \quad (73)$$

A_i is surmised from (73) and defined by

$$A_i = [I_{ci} / (V_c^2 \sigma_{i,\phi} \sigma_{i,E})] \cdot \left\{ 1 - e^{-(1/\sigma_{i,E})} - [\sigma_{i,\phi} / (\sigma_{i,\phi} - \sigma_{i,E})] \cdot \left[e^{-(1/\sigma_{i,\phi})} - e^{-(1/\sigma_{i,E})} \right] \right\}^{-1}. \quad (74)$$

Electron current is represented in

$$I_e(Y_{e,E}, Y_{e,\phi}) = A_e e^{[(Y_{e,E}-1)/\sigma_{e,E}]} e^{-(Y_{e,\phi}/\sigma_{e,\phi})} \quad (75)$$

and the circulating electron current is now defined by

$$I_{ce} = V_c^2 \int_{Y_{\min}}^1 dY_{e,E} \int_0^{Y_{e,E}-Y_{\min}} dY_{e,\phi} I_e(Y_{e,E}, Y_{e,\phi}). \quad (76)$$

Analogous to A_i , for the BCA system, a difficulty occurs in determining the value of A_e , for the BAC system, because ranges for the electron total and angular energies are $0 \leq Y_{e,\phi} \leq (Y_{e,E} - Y_{\min})$ and $Y_{\min} \leq Y_{e,E} \leq 1$. As in the case of the BCA system, this BAC system requires knowledge of the minimum normalized potential, which is information that we seek from the solution of (58). Thus, A_e is solved as a function of Y_{\min}

$$A_e(Y_{\min}) = [I_{ce} / (V_c^2 \sigma_{e,\phi} \sigma_{e,E})] \cdot \left\{ 1 - e^{((Y_{\min}-1)/\sigma_{e,E})} + [\sigma_{e,\phi} / (\sigma_{e,\phi} - \sigma_{e,E})] \cdot \left[e^{((Y_{\min}-1)/\sigma_{e,\phi})} - e^{((Y_{\min}-1)/\sigma_{e,E})} \right] \right\}^{-1} \quad (77)$$

Accurate values for A_e , and solutions to (58) are thus obtained by performing the same iterative procedure used to determine A_i , and obtain solutions to (48) for the BCA system.

In parallel with (65) and (70), for BCA systems, we obtain

$$F_i(X, Y) = \frac{K_i}{X^2} \int_0^Y dY_{i,E} \times \int_0^{X^2(Y-Y_{i,E})} dY_{i,\phi} \frac{e^{-(Y_{i,E}/\sigma_{i,E})} e^{-(Y_{i,\phi}/\sigma_{i,\phi})}}{[Y - Y_{i,E} - (Y_{i,\phi}/X^2)]^{1/2}} \quad (78)$$

and

$$G_e(X, Y) = \frac{K_e}{X^2} \int_Y^1 dY_{e,E} \times \int_0^{X^2(Y_{e,E}-Y)} dY_{e,\phi} \frac{e^{-(Y_{e,E}/\sigma_{e,E})} e^{-(Y_{e,\phi}/\sigma_{e,\phi})}}{[Y_{e,E} - Y - (Y_{e,\phi}/X^2)]^{1/2}}. \quad (79)$$

The values of K_i and K_e for (78) and (79), respectively, are defined as

$$K_i = [2\eta/(1 - \eta^2)] \cdot \{ [1/(4\pi\epsilon_0 \sigma_{i,E} \sigma_{i,\phi})] \cdot [m_i/(2e)]^{1/2} \} \cdot \left\{ 1 - e^{-(1/\sigma_{i,E})} - [\sigma_{i,\phi} / (\sigma_{i,\phi} - \sigma_{i,E})] \cdot \left[e^{-(1/\sigma_{i,\phi})} - e^{-(1/\sigma_{i,E})} \right] \right\}^{-1} \cdot (I_i/V_c^{3/2}) \quad (80)$$

and

$$K_e = [2\eta/(1 - \eta^2)] \cdot \{ [1/(4\pi\epsilon_0 \sigma_{e,E} \sigma_{e,\phi})] \cdot [m_e/(2e)]^{1/2} \} \cdot \left\{ 1 - e^{((Y_{\min}-1)/\sigma_{e,E})} + [\sigma_{e,\phi} / (\sigma_{e,\phi} - \sigma_{e,E})] \cdot \left[e^{((Y_{\min}-1)/\sigma_{e,\phi})} - e^{((Y_{\min}-1)/\sigma_{e,E})} \right] \right\}^{-1} \cdot (I_e/V_c^{3/2}) \quad (81)$$

where η is the transparency of the cathode.

TABLE II
SUMMARY OF THE SYSTEMS AND CORRESPONDING EQUATIONS

System	Model	Right Hand Side of Model
UCA	$\frac{1}{X^2} \frac{d}{dX} X^2 \frac{dY}{dX} = F_e(X, Y)$ (47)	Use $F_e(X, Y)$ in (85), with K_e in (66).
BCA	$\frac{1}{X^2} \frac{d}{dX} X^2 \frac{dY}{dX} = F_e(X, Y) - G_i(X, Y)$ (48)	Use $F_e(X, Y)$ in (85), with K_e in (66). Use $G_i(X, Y)$ in (82) with K_i in (71).
BAC	$\frac{1}{X^2} \frac{d}{dX} X^2 \frac{dY}{dX} = F_i(X, Y) - G_e(X, Y)$ (58)	Use $F_i(X, Y)$ in (86), with K_i in (80). Use $G_e(X, Y)$ in (83) with K_e in (81).

C. Method of Solution

Equations (47), (48), and (58) are solved numerically. The double integrals on the right hand sides of (65), (70), (78), and (79) have been previously evaluated by expanding the exponentials into Taylor Series. After Taylor series expansion, the integral of the resulting argument may be found using a standard table of integrals [14]. However, we have found that it is possible to express the double integrals on the right hand sides of (65), (70), (78), and (79) in terms of error functions for which fast and accurate numerical routines are readily available. Thus, for $G_i(X, Y)$ and $G_e(X, Y)$, we have

$$\begin{aligned}
 G_i(X, Y) &= (K_i/X) \cdot [(\pi^{1/2} \sigma_{i,E} \sigma_{i,\phi}) / (\sigma_{i,\phi} - \sigma_{i,E} X^2)] \\
 &\cdot \left\{ \sigma_{i,\phi}^{1/2} \cdot e^{[X^2(Y-1)/\sigma_{i,\phi}]} \cdot \text{Erfi} \left[X(1-Y)^{1/2} / \sigma_{i,\phi}^{1/2} \right] \right. \\
 &\left. - \sigma_{i,E}^{1/2} e^{[(Y-1)/\sigma_{i,E}]} \cdot X \cdot \text{Erfi} \left[(1-Y)^{1/2} / \sigma_{i,E}^{1/2} \right] \right\} \quad (82)
 \end{aligned}$$

and

$$\begin{aligned}
 G_e(X, Y) &= (K_e/X) \cdot [(\pi^{1/2} \sigma_{e,E} \sigma_{e,\phi}) / (\sigma_{e,\phi} - \sigma_{e,E} X^2)] \\
 &\cdot \left\{ \sigma_{e,\phi}^{1/2} \cdot e^{[X^2(Y-1)/\sigma_{e,\phi}]} \cdot \text{Erfi} \left[X(1-Y)^{1/2} / \sigma_{e,\phi}^{1/2} \right] \right. \\
 &\left. - \sigma_{e,E}^{1/2} e^{[(Y-1)/\sigma_{e,E}]} \cdot X \cdot \text{Erfi} \left[(1-Y)^{1/2} / \sigma_{e,E}^{1/2} \right] \right\} \quad (83)
 \end{aligned}$$

where $\text{Erfi}[z]$ is the imaginary error function, which is defined by

$$\text{Erfi}[z] = \frac{\text{Erf}[iz]}{i} \quad (84)$$

where $\text{Erf}[z]$ is the error function. Similarly for $F_e(X, Y)$ and $F_i(X, Y)$ we find

$$\begin{aligned}
 F_e(X, Y) &= (K_e/X) \cdot [(\pi^{1/2} \sigma_{e,E} \sigma_{e,\phi}) / (\sigma_{e,\phi} - \sigma_{e,E} X^2)] \\
 &\cdot \left\{ \sigma_{e,\phi}^{1/2} \cdot e^{-(X^2 Y / \sigma_{e,\phi})} \cdot \text{Erfi} \left[X Y^{1/2} / \sigma_{e,\phi}^{1/2} \right] \right. \\
 &\left. - \sigma_{e,E}^{1/2} e^{-(Y / \sigma_{e,E})} \cdot X \cdot \text{Erfi} \left[Y^{1/2} / \sigma_{e,E}^{1/2} \right] \right\} \quad (85)
 \end{aligned}$$

$$\begin{aligned}
 F_i(X, Y) &= (K_i/X) \cdot [(\pi^{1/2} \sigma_{i,E} \sigma_{i,\phi}) / (\sigma_{i,\phi} - \sigma_{i,E} X^2)] \\
 &\cdot \left\{ \sigma_{i,\phi}^{1/2} \cdot e^{-(X^2 Y / \sigma_{i,\phi})} \cdot \text{Erfi} \left[X Y^{1/2} / \sigma_{i,\phi}^{1/2} \right] \right. \\
 &\left. - \sigma_{i,E}^{1/2} e^{-(Y / \sigma_{i,E})} \cdot X \cdot \text{Erfi} \left[Y^{1/2} / \sigma_{i,E}^{1/2} \right] \right\} \quad (86)
 \end{aligned}$$

These results dramatically reduce computational labor and increase computational speed.

Equations (82), (83), (85), and (86) can be inserted into (47), (48) and (58). The latter equations are then solved numerically by using the boundary condition in (52) and employing the shooting method to determine the value of $Y(0)$ that satisfies (51). The models just described, for each of the systems in Table I, are summarized in Table II.

D. Double Well Definitions

In order to study double well solutions for (48) and (58), it is convenient to introduce some measures. Using the terminology of Momota and Miley [26], we will describe single potential well structures, such as those produced by UCA systems, as potential hills. In the bipolar systems, the second potential well of opposite polarity that forms within the potential hill will be termed as a potential well. Thus, double well structures will be described as potential wells forming within potential hills. A central potential well will provide better confinement as the depth of the potential well increases. We introduce the quantity “double well depth” (DWD) is defined by Tzonev [31], and depicted in Fig. 8

$$\text{DWD} = \frac{Y_{\text{peak}} - Y_{\text{min}}}{1 - Y_{\text{min}}} \quad (87)$$

The width of a potential well is also depicted in Fig. 8, and is defined as the full width at half maximum (FWHM). The value of half-maximum is the average of the peak potential of the potential well and the potential associated with the “height” of the potential hill. The FWHM is a measure of the volume available for fusion reactions to take place, if they are assumed to take place within a spherical region at the center of the device.

III. RESULTS

A. Comparison With Hirsch's Results

Hirsch calculated many solutions to (19), and determined what values of K_i and λ_i were necessary for the formation of multiple potential well structures within the cathode of a BAC

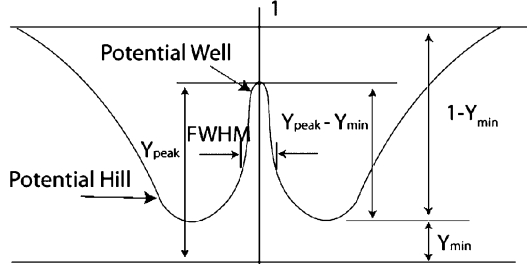
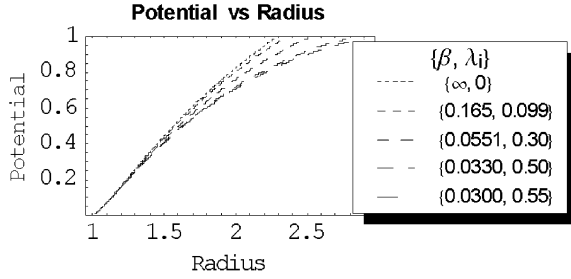
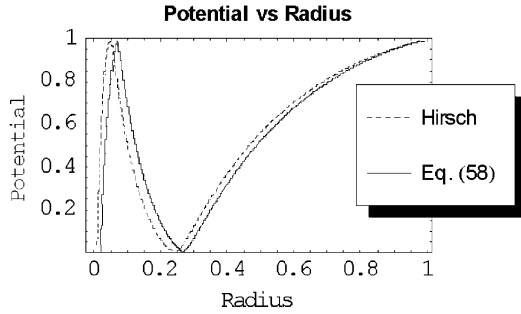


Fig. 8. Depiction of a typical double well solution.

Fig. 9. Depicted are solutions to (58), in the limit that energy spreads are negligible, for many values of β . These may be compared to solutions of (19) computed by Hirsch [13] for several values of λ_i .Fig. 10. Multiple potential well solutions are depicted for (58), in the limit that energy spreads are negligible, and for Hirsch's model [13], (19). These solutions are calculated for $K_i = 0.7$, and $\lambda_i = 0.45$.

device. Generally, for a given K_i Hirsch found that multiple potential well structures should exist for all $\lambda_i \leq \lambda_{i,\max}$, where $\lambda_{i,\max}$ is the maximum value of λ_i for which multiple well solutions may exist. In addition, as K_i increased, the value of $\lambda_{i,\max}$ was also seen to increase. In particular, for $K_i = 1$, Hirsch found $\lambda_{i,\max} \approx 0.55$. Solutions to (58), are compared by relating the ion perveance to K_i and relating λ_i to β , with

$$P_i = K_i \left(\frac{2e}{m_i} \right)^{1/2} \quad (88)$$

and

$$\beta = (\lambda_i)^{-1} \left(\frac{m_e}{m_i} \right)^{1/2}. \quad (89)$$

In (58), values for the spreads in the total and angular energies of electrons and ions (i.e., $\sigma_{e,E}$, $\sigma_{e,\phi}$, $\sigma_{i,E}$, and $\sigma_{i,\phi}$) are made very small, $\approx 1 \times 10^{-6}$ in order to compare solutions of (58) to solutions of Hirsch's model [13], (19), for $K_i = 1$. These solutions are provided in the Fig. 9. Next, a multiple potential well structure is computed for the BAC SIEC, from (58), and compared to a multiple well solution computed by Hirsch [13]

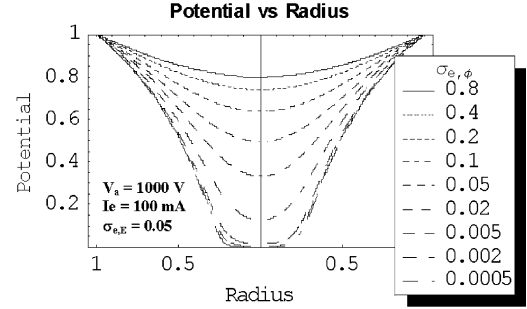


Fig. 11. Potential versus Radius for the UCA model as a function of angular energy spread.

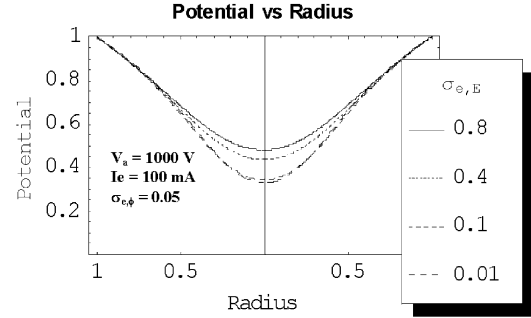


Fig. 12. Potential versus Radius for the UCA model as a function of total energy spread.

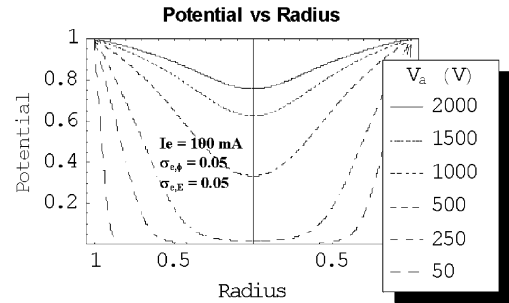


Fig. 13. Potential versus Radius for the UCA model as a function of applied voltage.

with $K_i = 0.7$, and $\lambda_i = 0.45$. These results are provided in Fig. 10.

B. Parametric Study of UCA SIEC

Solutions for the UCA SIEC are calculated from (47). The solutions for different values of $\sigma_{e,E}$, $\sigma_{e,\phi}$, I_e , and V_a are shown in Figs. 11–14. Fig. 11 shows several solutions to the UCA model for values of $\sigma_{e,\phi}$ over the range of $0.0005 \leq \sigma_{e,\phi} \leq 0.8$. Solutions, for multiple values of $\sigma_{e,E}$, where $0.01 \leq \sigma_{e,E} \leq 0.8$ are shown in Fig. 12. Fig. 13 contains solutions for UCA model as the voltage is varied from $50 \leq V_a \leq 2000$ V, while Fig. 14 contains solutions for several values of current, with $25 \leq I_e \leq 375$ mA.

C. Parametric Study of BCA SIEC

Each one of the parameters, $\sigma_{e,\phi}$, $\sigma_{e,E}$, $\sigma_{i,\phi}$, $\sigma_{i,E}$, P_e , η , and β , are varied, while the rest are held constant to observe trends in the solution of (48). Fig. 15 shows solutions for the BCA system

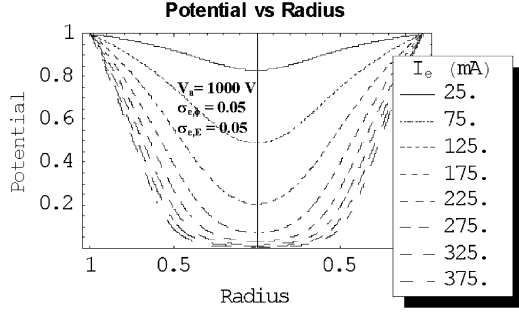


Fig. 14. Potential versus Radius for the UCA model as a function of current.

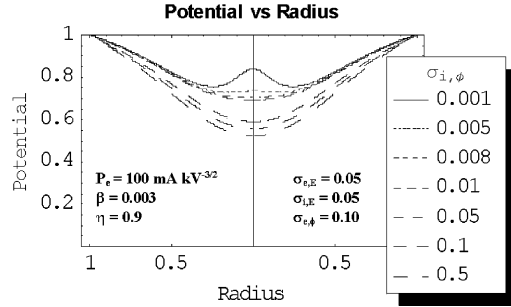


Fig. 15. Potential versus Radius for the BCA model as a function of ion angular energy spreads.

TABLE III
DWD AND FWHM FOR THE BCA MODEL, FOR SEVERAL VALUES OF ION ANGULAR ENERGY SPREAD, AS SHOWN IN FIG. 15

$\sigma_{i,\phi}$	Y_{\min}	Y_{peak}	DWD	FWHM
0.001	0.753	0.835	0.333	0.206
0.005	0.730	0.736	0.024	0.171
0.008	0.708	0.708	-	-
0.010	0.695	0.695	-	-
0.050	0.590	0.590	-	-
0.100	0.555	0.555	-	-
0.500	0.521	0.521	-	-

for various values of $\sigma_{i,\phi}$ in the range $0.001 \leq \sigma_{i,\phi} \leq 0.5$, and Table III provides a list of their FWHMs and DWDs. Fig. 16 contains several solutions for $\sigma_{i,E}$ over $0.01 \leq \sigma_{i,E} \leq 0.8$, with the FWHM and DWD of each solution listed in Table IV. Electron angular energy is varied from $0.01 \leq \sigma_{e,\phi} \leq 0.15$ and solutions for these values are given in Fig. 17, with the associated FWHM and DWD data provided in Table V. Next, solutions for $\sigma_{e,E}$ over $0.05 \leq \sigma_{e,E} \leq 0.8$ are shown in Fig. 18, and the FWHMs and DWDs for these solutions are given in Table VI. The ratio of ion current to electron current β is varied for $0 \leq \beta \leq 0.003$ and solutions are given in Fig. 19, while the FWHM and DWD data for these solutions are given in Table VII. The electron perveance is varied for $140 \leq P_e \leq 395 \text{ mA/kV}^{3/2}$ and solutions are given in Fig. 20, with a list of the FWHMs and DWDs given in Table VIII. Finally, (48) is solved for several values of grid transparency, $0.83 \leq \eta \leq 0.94$, and the solutions are displayed in Fig. 21, with a list of the FWHMs and DWDs provided in Table IX.

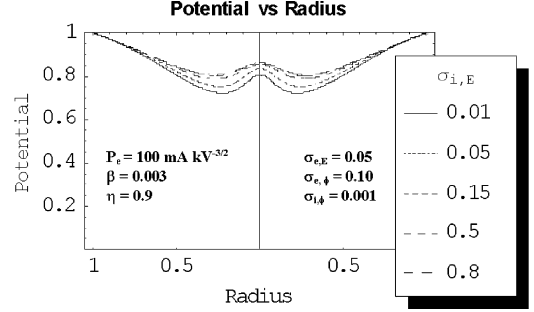


Fig. 16. Potential versus Radius for the BCA model as a function of ion total energy spreads.

TABLE IV
DWD AND FWHM FOR THE BCA MODEL, FOR SEVERAL VALUES OF ION TOTAL ENERGY SPREAD, AS SHOWN IN FIG. 16

$\sigma_{i,E}$	Y_{\min}	Y_{peak}	DWD	FWHM
0.010	0.721	0.805	0.302	0.181
0.050	0.753	0.835	0.332	0.205
0.150	0.789	0.854	0.310	0.234
0.500	0.804	0.860	0.285	0.246
0.800	0.806	0.860	0.280	0.248

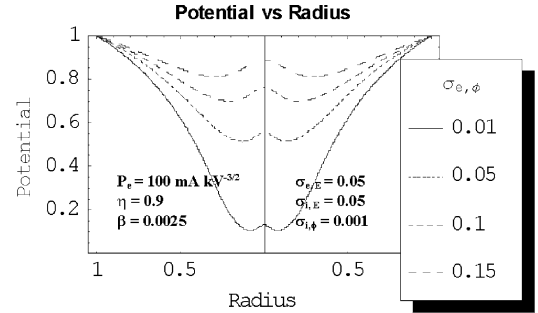


Fig. 17. Potential versus Radius for the BCA model as a function of electron angular energy spreads.

TABLE V
DWD AND FWHM FOR THE BCA MODEL, FOR SEVERAL VALUES OF ELECTRON ANGULAR ENERGY SPREAD, AS SHOWN IN FIG. 17

$\sigma_{e,\phi}$	Y_{\min}	Y_{peak}	DWD	FWHM
0.010	0.106	0.129	0.025	0.075
0.050	0.515	0.555	0.082	0.116
0.100	0.700	0.762	0.207	0.173
0.15	0.812	0.888	0.402	0.251

D. Parametric Study of BAC SIEC

Each one of the parameters, $\sigma_{e,\phi}$, $\sigma_{e,E}$, $\sigma_{i,\phi}$, $\sigma_{i,E}$, P_i , η , and β , is varied, with the rest held constant to observe trends in the solution of (58) for the BAC system. Fig. 22 shows solutions for the BAC system for various values of $\sigma_{e,\phi}$ in the range $0.0005 \leq \sigma_{e,\phi} \leq 0.1$ and Fig. 23 contains several solutions for $\sigma_{e,E}$ over $0.01 \leq \sigma_{e,E} \leq 0.5$. Ion angular energy is varied from $0.06 \leq \sigma_{i,\phi} \leq 0.18$ and solutions for these values are given in Fig. 24. Next, solutions for $\sigma_{i,E}$ over $0.01 \leq \sigma_{i,E} \leq 0.3$ are shown in Fig. 25. β is varied for $0.2 \leq \beta \leq 1.25$ and solutions are given in Fig. 26, and the ion perveance is varied for $0.81 \leq P_i \leq 4.5 \text{ mA/kV}^{3/2}$ with solutions given in Fig. 27. Finally, (58) is solved for many values of the grid transparency from $0.83 \leq$

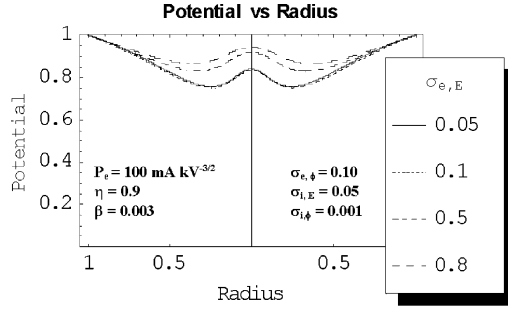


Fig. 18. Potential versus Radius for the BCA model as a function of total electron energy spreads.

TABLE VI
DWD AND FWHM FOR THE BCA MODEL, FOR SEVERAL VALUES OF ELECTRON TOTAL ENERGY SPREAD, AS SHOWN IN FIG. 18

$\sigma_{e,E}$	Y_{min}	Y_{peak}	DWD	FWHM
0.050	0.756	0.839	0.338	0.208
0.100	0.752	0.837	0.342	0.209
0.500	0.832	0.919	0.520	0.289
0.800	0.865	0.943	0.580	0.336

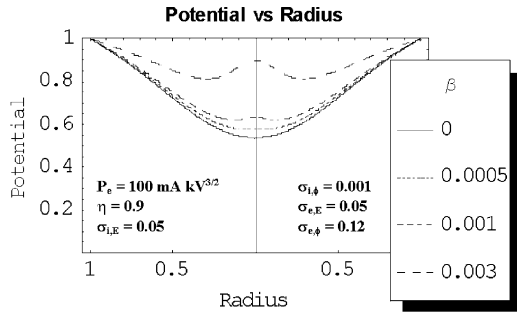


Fig. 19. Potential versus Radius for the BCA model as a function of β .

TABLE VII
DWD AND FWHM FOR THE BCA MODEL FOR SEVERAL VALUES OF β , AS SHOWN IN FIG. 19

β	Y_{min}	Y_{peak}	DWD	FWHM
0	0.535	0.535	-	-
0.0005	0.580	0.583	0.006	0.080
0.001	0.620	0.633	0.036	0.117
0.003	0.813	0.898	0.453	0.254

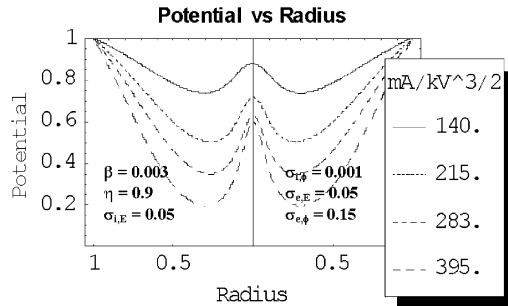


Fig. 20. Potential versus Radius for the BCA model as a function of P_e .

$\eta \leq 0.94$, and the solutions are displayed in Fig. 28. FWHM and DWD data for the solutions in Figs. 22–28 are provided in Tables X–XVI.

TABLE VIII
DWD AND FWHM FOR THE BCA MODEL FOR SEVERAL VALUES OF P_e , AS SHOWN IN FIG. 20

P_e (mA kV ^{-3/2})	Y_{min}	Y_{peak}	DWD	FWHM
140	0.736	0.876	0.530	0.244
215	0.502	0.719	0.435	0.186
283	0.349	0.630	0.432	0.174
395	0.198	0.597	0.498	0.173

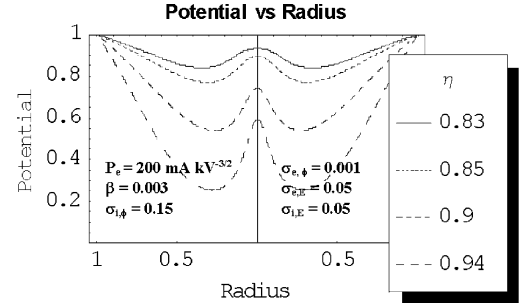


Fig. 21. Potential versus Radius for the BCA model as a function of anode transparency, η .

TABLE IX
DWD AND FWHM FOR THE BCA MODEL FOR SEVERAL VALUES OF η , AS SHOWN IN FIG. 21

η	Y_{min}	Y_{peak}	DWD	FWHM
0.83	0.840	0.934	0.588	0.310
0.85	0.771	0.896	0.547	0.261
0.90	0.540	0.742	0.439	0.191
0.94	0.254	0.595	0.457	0.171

IV. DISCUSSION

The reliability of this method is illustrated by the results in Figs. 9 and 10. Equation (58) is solved using $F_i(X, Y)$ and $G_e(X, Y)$ as given by (86) and (83), respectively, for Figs. 9 and 10. In Fig. 9, it is found that for a value of $P_i = 3.79$ mA/kV^{3/2} ($K_i = 1.0$), the solution of (58) is nearly tangent to the $Y = 1$ axis for $\beta = 0.003$ ($\lambda_i = 0.55$). This agrees well with results presented by Hirsch [13], in which it was computed that $\lambda_{i,max} = 0.55$ for $K_i = 1.0$. Fig. 10 depicts solutions to (19) and (58) for negligible energy spreads. The good agreement between the two curves adds further confidence to the results computed by the method for BAC SIECs in Table II.

Further verification of the method may be achieved by comparing solutions for the UCA case to solutions computed by Swanson [30]. Fig. 11 shows that the solution is highly dependent on the angular energy spread, and, as the angular energy spread of electrons decreases, the solution of (47) approaches the solution of Langmuir and Blodgett [18] in Fig. 1. Variation in the total energy spread of electrons has very little effect on the potential well shape as indicated in Fig. 12. Figs. 13 and 14 show that potential well depth varies proportionally to the electron permeance, P_e .

Considering the BCA solutions, Figs. 15–21 and Tables III–IX show that a double well solution depends most greatly on the value of $\sigma_{i,\phi}$. A double well structure exists for small values of $\sigma_{i,\phi}$, and vanishes rapidly as $\sigma_{i,\phi}$ is increased.

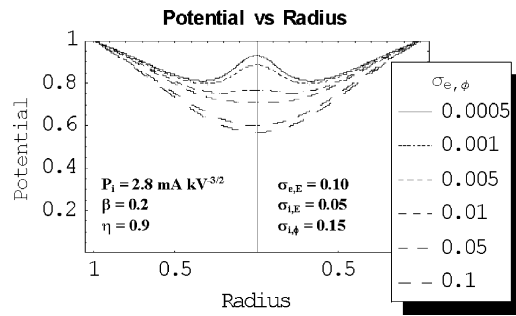


Fig. 22. Potential versus Radius for the BAC model as a function of spread in angular electron energy.

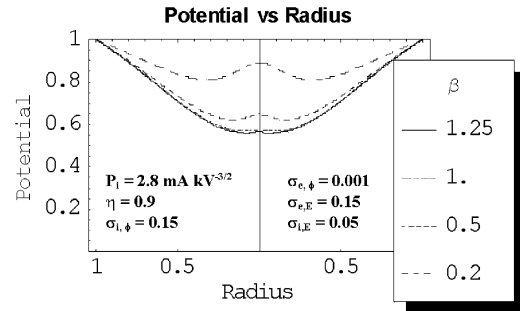


Fig. 26. Potential versus Radius for the BAC model as a function of β .

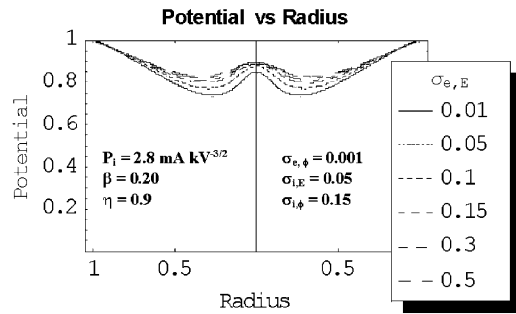


Fig. 23. Potential versus Radius for the BAC model as a function of spread in total electron energy.

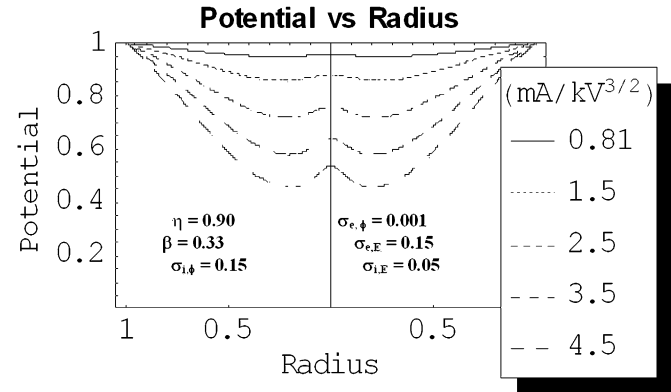


Fig. 27. Potential versus Radius for the BAC model as a function of ion permeance.

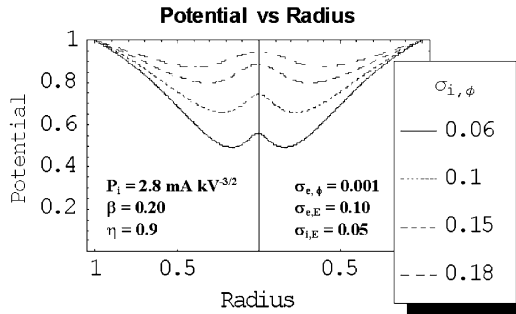


Fig. 24. Potential versus Radius for the BAC model as a function of spread in angular ion energy.

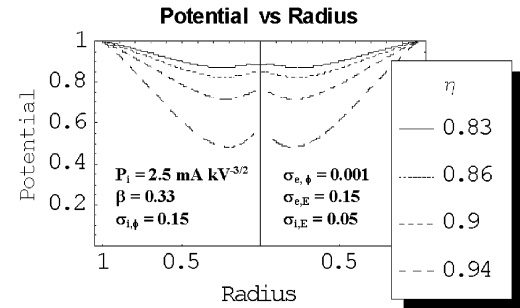


Fig. 28. Potential versus Radius for the BAC system as a function η .

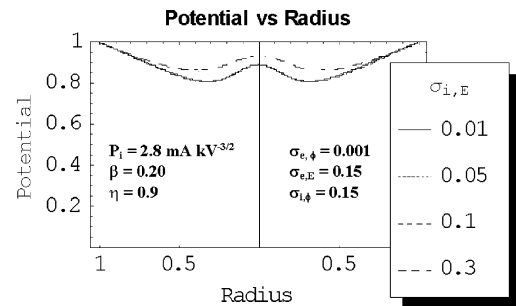


Fig. 25. Potential versus Radius for the BAC model as a function of spread in total ion energy.

Small values of $\sigma_{e,\phi}$ tend to “increase the height” of the potential hill. The value of $\sigma_{i,E}$ has a noticeable effect on the central potential well, but the double well solution does not vanish nearly as rapidly for increasing values of $\sigma_{i,E}$ as it does for increasing values of $\sigma_{i,\phi}$. In fact, double well solutions still exist for relatively large values of $\sigma_{i,E}$. The value of $\sigma_{e,E}$

TABLE X
DWD AND FWHM FOR THE BAC MODEL FOR SEVERAL VALUES OF ELECTRON ANGULAR ENERGY SPREAD, AS SHOWN IN FIG. 22.

$\sigma_{e,\phi}$	Y_{\min}	Y_{peak}	DWD	FWHM
0.0005	0.810	0.928	0.620	0.272
0.001	0.798	0.887	0.441	0.272
0.005	0.754	0.767	0.053	0.228
0.010	0.713	0.713	-	-
0.050	0.603	0.603	-	-
0.100	0.570	0.569	-	-

may also have an impact on the solution to (48). However, as Fig. 18 illustrates, double well solutions still survive for large values of $\sigma_{e,E}$. Fig. 20 and Table VIII reveal that the DWD is proportional to P_e . Finally, Fig. 21, and the data in Table IX show that the “height” of the potential hill “increases” as the transparency of the anode increases. In addition, the absolute depth of the potential well, with respect to the anode grid potential, also increases.

TABLE XI
DWD AND FWHM FOR THE BAC MODEL FOR SEVERAL VALUES OF
ELECTRON TOTAL ENERGY SPREAD, AS SHOWN IN FIG. 23.

$\sigma_{e,E}$	Y_{min}	Y_{peak}	DWD	FWHM
0.01	0.737	0.848	0.422	0.209
0.05	0.771	0.876	0.460	0.244
0.10	0.798	0.887	0.441	0.272
0.15	0.809	0.890	0.425	0.283
0.30	0.822	0.894	0.405	0.295
0.50	0.827	0.896	0.397	0.300

TABLE XII
DWD AND FWHM FOR THE BAC MODEL FOR SEVERAL VALUES OF ION
ANGULAR ENERGY SPREAD, AS SHOWN IN FIG. 24.

$\sigma_{i,\phi}$	Y_{min}	Y_{peak}	DWD	FWHM
0.06	0.493	0.557	0.126	0.133
0.10	0.659	0.742	0.245	0.183
0.15	0.798	0.887	0.441	0.272
0.18	0.874	0.945	0.562	0.367

TABLE XIII
DWD AND FWHM FOR THE BAC MODEL FOR SEVERAL VALUES OF ION
TOTAL ENERGY SPREAD, AS SHOWN IN FIG. 25.

$\sigma_{i,E}$	Y_{min}	Y_{peak}	DWD	FWHM
0.01	0.812	0.891	0.421	0.282
0.05	0.810	0.890	0.425	0.283
0.10	0.810	0.892	0.434	0.288
0.30	0.864	0.936	0.528	0.360

TABLE XIV
DWD AND FWHM FOR THE BAC MODEL FOR SEVERAL VALUES
OF β , AS SHOWN IN FIG. 26.

β	Y_{min}	Y_{peak}	DWD	FWHM
1.250	0.558	0.561	0.007	0.086
1.000	0.569	0.575	0.012	0.099
0.500	0.623	0.646	0.061	0.143
0.200	0.809	0.890	0.425	0.283

TABLE XV
DWD AND FWHM FOR THE BAC MODEL FOR SEVERAL VALUES
OF P_i , AS SHOWN IN FIG. 27.

P_i (mA kV ^{-3/2})	Y_{min}	Y_{peak}	DWD	FWHM
0.81	0.947	0.953	0.103	0.273
1.5	0.859	0.878	0.136	0.225
2.5	0.719	0.758	0.142	0.186
3.5	0.579	0.640	0.144	0.166
4.5	0.456	0.536	0.148	0.155

TABLE XVI
DWD AND FWHM FOR THE BAC MODEL FOR SEVERAL VALUES
OF η , AS SHOWN IN FIG. 28.

η	Y_{min}	Y_{peak}	DWD	FWHM
0.83	0.871	0.888	0.135	0.230
0.86	0.825	0.849	0.139	0.213
0.90	0.719	0.759	0.142	0.186
0.94	0.483	0.559	0.147	0.157

If BAC solutions are now considered, in Fig. 22, it is evident that the existence of a double well structure depends rather strongly on $\sigma_{e,\phi}$ since the central peak in Fig. 22 vanishes rapidly as the angular energy of the electrons increases. The

“height” of the potential hill increases substantially for decreasing values of $\sigma_{i,\phi}$, in Fig. 24, but the DWD of the solution is also degraded. Fig. 23 shows that the DWD of the potential well is generally degraded for increasing values of $\sigma_{e,E}$. Fig. 25 reveals that the value of $\sigma_{i,E}$ has minimal a effect on the potential well structure, while Fig. 27 reveals that the DWD of a potential well varies with proportion to the ion perveance, P_i . Finally, Fig. 28 and Table XVI show that the “height” of the potential hill and the DWD of the potential well both increases as the transparency of the cathode grid increases.

The solutions for BCA and BAC SIECs, just presented, support, and extend the conclusion drawn by Momota and Miley [26], that improving the relative focusing of electrons to ions, for BAC SIECs, will increase the DWD of the potential well. It is extended here to BCA SIECs as well, where the conclusion may be drawn from the results in Figs. 15–18 and Tables III–IX that the DWD of the potential well will increase as the relative focusing of ions to electrons is increased. The conclusion drawn by Momota and Miley may be generalized for the BCA and BAC systems, in Table I, by stating that the DWD of bipolar SIECs increases as the relative focusing of the secondary particle to the primary particle improves.

The relationship between the results for the BAC SIEC and experimental results can be determined by considering the solutions in Fig. 27 and Table XV. Gu [17] observed the evolution of a double potential well profile in a BAC SIEC using a high-resolution proton collimator. He observed the appearance of a double well structure for $P_i \geq 0.34$ mA/kV^{3/2}, and observed that the DWD of the potential well increased as P_i was increased. Fig. 27 and Table XV support Gu’s experimental observations, as these results indicate that the DWD increases with increasing P_i . However, we are unable to determine exactly at what perveance double wells begin to form, because solutions do not converge for ion perveance values $P_i < 0.81$ mA/kV^{3/2}. Any discrepancy between the results presented here, and experimental results is not surprising since collisions are neglected in the model described by (58). In addition, the actually energy distribution within SIECs is unknown, and little effort is made here to ensure that the shape of the energy distributions used in these calculations accurately describes the shape of energy distributions in experimental devices.

The fact that significant neutron outputs are reported for experiments operating at $P_i < 1$ suggests deep potential hills may not be necessary for fusion reactions. Since potential hill depth is an indication of ion convergence, then neutron productions at shallow potential hills suggests that ion-neutral, not ion-ion collisions are responsible for the majority of fusion reactions in IEC devices. Of course, it is also possible that potential hills of appreciable depth do form in these experiments. If this is the case, then it would indicate (according to the discussion in Section 1.D) that ion sources in experimental devices are more beam-like than the simulations in Fig. 27, perhaps due to “star-mode” operation.

V. SUMMARY AND CONCLUSION

IEC devices could provide a very compact portable source of neutrons for NAA applications. Their small size also makes

them attractive candidates for powering spacecraft, if IEC's ever achieve an energy gain greater than unity. Hirsch [13] reported detecting neutron rates of 10^8 D-D or 10^{10} D-T n/s from an ion-injected (BAC) device. It was postulated that the mechanism responsible for such high fusion rates was the formation of multiple virtual electrodes at the center of the device. The results of experimental and theoretical efforts aimed at validating or negating the multiple virtual electrode hypothesis, have so far been nondefinitive.

Collisionless models are derived to describe UCA, BCA, and BAC systems in steady state, based on previous work by Lavrent'ev, Dolan, and Swanson [19]–[21]. The resulting integral equations are solved in a unique way, and an extensive parametric study is performed on all systems and the conditions most conducive to double well formation are delineated. The method is validated by comparing solutions computed for the UCA SIEC to solutions previously computed by Swanson [30]. Further validation is achieved by benchmarking the method for the BAC SIEC against Hirsch's solutions in the limiting case that energy spreads of electrons and ions are negligible.

Results for the BCA and BAC SIECs allow us to generalize the conclusion of Momota and Miley [26] in prior computations. The DWD of a potential well increases as the relative focusing of the secondary particle to the primary particle increases. In addition, computations for the BAC SIEC generally agree with experiments performed by Gu [17]. In both Gu's experiments, and the calculations performed in this work, it is observed that the DWD of a potential well increases as the ion perveance, P_i , increases. However, shortcomings to our model, such as the absence of collisions and unverified energy distribution functions limit how well these simulations match experimental observation. The shortcomings of this model indicate that much work is still required to accurately model experimental SIEC devices. However, given the good agreement between this work, and prior collisionless models, and the extensive set of solutions computed, these simulations provide a valuable benchmark for studying trends in IEC behavior.

ACKNOWLEDGMENT

The authors would like to acknowledge the advice and encouragement by faculty of the Nuclear Science and Engineering Institute, and the Electrical Engineering Department of the University of Missouri-Columbia.

REFERENCES

- [1] L. Chacon and G. H. Miley, "Inertial electrostatic confinement ^3He breeder for D- ^3He satellite systems," *Fusion Technol.*, vol. 33, p. 182, Mar. 1998.
- [2] B. Bromley, "Approximate modeling of the inertial electrostatic confinement cylindrical device," M.S. thesis, Univ. Illinois, Urbana-Champaign, IL, 1997.
- [3] J. B. Javedani, Y. B. Gu, M. J. Williams, J. Hartwell, R. L. Anderl, G. H. Miley, J. H. Nadler, J. L. Jones, R. A. Nebel, and D. C. Barnes, "Studies of the IEC accelerator-plasma target fusion neutron source for activation analysis," *Bull. Amer. Phys. Soc.*, vol. 39, no. 7, p. 1768, 1994.
- [4] G. H. Miley and H. Momota, "A collimator-converter system for IEC propulsion," *Space Technol. Appl. Int. Forum-STAIF 2002*, pp. 768–779, 2002.
- [5] G. H. Miley, R. Burton, H. Momota, N. Richardson, M. Coventry, and Y. Shaban, "High performance manned interplanetary space vehicle using D- ^3He inertial electrostatic fusion," *Space Technol. Appl. Int. Forum-STAIF 2002*, pp. 819–827, 2002.
- [6] R. W. Bussard, "An advanced fusion energy system for outer-planet space propulsion," *Space Technol. Appl. Int. Forum-STAIF 2002*, pp. 768–779, 2002.
- [7] J. W. Weidner, "The Production of ^{13}N from inertial electrostatic confinement fusion," M.S. thesis, Univ. Wisconsin, Madison, WI, 2003.
- [8] J. W. Weidner, G. L. Kulcinski, J. F. Santarius, R. P. Ashley, G. Piefer, B. Cipiti, R. Radel, and S. K. Murali, "Production of ^{13}N via inertial electrostatic confinement fusion," *Fusion Sci. Technol.*, vol. 44, p. 539, 2003.
- [9] G. H. Miley, H. Momota, Y. Shaban, and H. Hora, "Progress in development of a converging veam neutron source for driving a sub-critical fission reactor," in *Proc. 10th Int. Conf. Nucl. Eng.*, Arlington, VA, Apr. 14–18, 2002.
- [10] W. M. Nevins, "Can inertial electrostatic confinement work beyond the ion-ion collisional time scale?," *Phys. Plasmas*, vol. 2, no. 10, p. 3804, Oct. 1995.
- [11] T. H. Rider, "A general critique of inertial-electrostatic confinement fusion systems," *Phys. Plasmas*, vol. 2, no. 6, p. 1853, Jun. 1995.
- [12] B. Jurczyk, "Theory and development of a sealed deuterium-tritium inertial electrostatic confinement neutron generator," M.S. thesis, Univ. Illinois, Urbana-Champaign, IL, 1997.
- [13] R. L. Hirsch, "Inertial electrostatic confinement of ionized fusion gases," *J. Appl. Phys.*, vol. 38, p. 4522, Oct. 1967.
- [14] D. A. Swanson, B. E. Cherrington, and J. T. Verdeyen, "Multiple potential-well structure created by electron injection in spherical geometry," *J. Appl. Phys. Lett.*, vol. 23, p. 125, Aug. 1973.
- [15] J. H. Nadler, "Space-charge dynamics and neutron generation in an inertial-electrostatic confinement device," Ph.D. dissertation, Univ. Illinois, Urbana-Champaign, 1992.
- [16] T. A. Thorson, R. D. Durst, R. J. Fonck, and L. P. Wainwright, "Convergence electrostatic potential, and density measurement in a spherical convergent ion focus," *Phys. Plasmas*, vol. 4, no. 1, p. 4, Jan. 1997.
- [17] Y. Gu and G. H. Miley, "Experimental study of potential structure in a spherical IEC fusion device," *IEEE Trans. Plasma Sci.*, vol. 28, no. 1, pp. 331–346, Feb. 2000.
- [18] I. Langmuir and K. E. Blodgett, "Currents limited by space charge between concentric spheres," *Phys. Rev.*, vol. 24, p. 49, 1924.
- [19] O. A. Lavrent'ev, "Investigation of an electromagnetic trap," *AEC-tr-7002*, 1970.
- [20] T. J. Dolan, "Electrostatic-inertial plasma confinement," Ph.D. dissertation, Univ. Illinois, Urbana-Champaign, 1975.
- [21] D. A. Swanson, "Theoretical study of a spherical inertial electrostatic plasma confinement device," Ph.D. dissertation, Univ. Illinois, Urbana-Champaign, 1975.
- [22] R. W. Hockney, "Formation and stability of virtual electrodes in a cylinder," *J. Appl. Phys.*, vol. 39, no. 9, p. 4166, Aug. 1968.
- [23] W. Black and E. H. Klevans, "Theory of potential-well formation in an electrostatic confinement device," *J. Appl. Phys.*, vol. 45, no. 6, p. 2502, June 1974.
- [24] K. M. Hu and E. H. Klevans, "On the theory of electrostatic confinement of plasmas with ion injection," *Phys. Fluids*, vol. 17, no. 1, p. 227, Jan. 1974.
- [25] H. Matsuura, T. Takaki, Y. Nakao, and K. Kudo, "Radial profile of neutron production rate in spherical inertial electrostatic confinement plasmas," *Fusion Technol.*, vol. 39, p. 1167, May 2001.
- [26] H. Momota and G. H. Miley, "Virtual cathode in a stationary spherical inertial electrostatic confinement," *Fusion Sci. Technol.*, vol. 40, p. 56, Jul. 2001.
- [27] M. Ohnishi and K. H. Sato, "Correlation between potential well structure and neutron production in inertial electrostatic confinement fusion," *Nucl. Fusion*, vol. 37, no. 5, p. 611, 1997.
- [28] P. T. Farnsworth, "Electric discharge device for producing interactions between nuclei," U.S. Patent 3 258 402, Jun. 1966.
- [29] T. J. Dolan, J. T. Verdeyen, D. J. Meeker, and B. E. Cherrington, "Electrostatic-inertial plasma confinement," *J. Appl. Phys.*, vol. 43, no. 4, p. 1590, Apr. 1972.
- [30] D. A. Swanson, B. E. Cherrington, and J. T. Verdeyn, "Recent developments in electrostatic confinement-theoretical," *Ann. NY Acad. Sci.*, p. 139, 1973.
- [31] I. V. Tzonev, "Effect of large ion angular momentum spread and high current on inertial electrostatic confinement potential structures," M.S. thesis, Univ. Illinois, Urbana-Champaign, 1996.



Ryan M. Meyer (M'00) received the B.S. degree in electrical engineering and the M.S. degree in nuclear engineering, in 2002 and 2004, respectively, from the University of Missouri-Columbia, where he is currently working toward the Ph.D. degree in nuclear engineering.

His research has been focused on theoretical and experimental studies of IEC devices.

Mr. Meyer has been a recipient of the U.S. Department of Education GAANN Fellowship, the University of Missouri Huggin's Graduate Fellowship, and the Missouri Space Grant Consortium (MSGC) Fellowship.



Sudarshan K. Loyalka received the B.S. degree from the University of Rajasthan, Rajasthan, India, in 1964, and the M.S. and Ph.D. degrees from Stanford University, Stanford, CA, in 1965 and 1967, respectively.

He is a Curators' Professor of Nuclear Engineering and Chemical Engineering at the University of Missouri-Columbia. His research and teaching interests are in the areas of aerosol mechanics, rarefied gas dynamics, and nuclear reactor physics and safety. At the University of Missouri-Columbia he has been director of their Particulate Systems Research Center since its inception in 1985.

He is a coauthor of three books.

Dr. Loyalka was elected a Fellow of the American Institute of Physics in 1982 for his contributions to understandings of the role of gas-surface interactions on transport processes. He was also elected a Fellow of the American Nuclear Society in 1985 for his contributions to aerosol mechanics, transport theory, nuclear reactor physics and safety, and education of nuclear engineers. He received the David Sinclair Award of the American Association of Aerosol Research in 1995 for his sustained outstanding research in aerosol science and technology, and the Glenn Murphy Award of the American Society for Engineering Education in 1998 for education of nuclear engineers.



Mark A. Prelas received the Ph.D. degree from the University of Illinois, Urbana-Champaign, in 1979.

He is H. O. Croft Professor of nuclear engineering at the University of Missouri-Columbia. In addition to being a Professor at the University of Missouri, he has worked at the U.S. Department of State in the bureau of Arms Control in 1999–2000, and with the Idaho National Engineering Laboratory of the U.S. Department of Energy in 1987. He has worked in the areas of arms control for weapons of mass destruction, the strategic defense initiative, the development of nuclear, chemical, and biological sensors, the synthesis and applications of wide bandgap materials, directed energy weapons, direct energy conversion and electronics. He has published over 200 papers, five books and holds 12 national and international patents.

Dr. Prelas received the Presidential Young Investigator Award in 1984, was a Gas Research Institute Fellow in 1981, was a Fulbright Fellow at the University of New South Wales in 1992, was named a fellow of the American Nuclear Society in 1999, and was a William C. Foster Fellow with the U.S. Department of State in 1999–2000.